Wnt target IQGAP3 promotes Wnt signaling via disrupting Axin1-CK1α interaction.

Muhammad Bakhait Rahmat[1, *], Aashiq Hussain[1], Teh Yu Xuan[1], Bibek Dutta[1], Sumedha Pundrik[1], Dennis Kappei[1,2,3], Yoshiaki Ito[1, *]

[1]Cancer Science Institute of Singapore, National University of Singapore, Singapore.

[2]Department of Biochemistry, Yong Loo Lin School of Medicine, National University of Singapore, Singapore

[3]NUS Center for Cancer Research, Yong Loo Lin School of Medicine, National University of Singapore, Singapore

*Correspondence:

Yoshiaki Ito, Cancer Science Institute of Singapore, NUS Centre for Cancer Research, Yong Loo Lin School of Medicine, National University of Singapore, 14 Medical Drive #12-01, Singapore 117599. Tel: +65-6516-2242, Fax: +65-6873-9664, email: yoshi_ito@nus.edu.sg.

Muhammad Bakhait Rahmat, email: csimbr@nus.edu.sg or bhitihd@hotmail.com.

ABSTRACT

The scaffold protein IQGAP3 is highly upregulated in most epithelial cancers. While recent studies have highlighted its pivotal roles in cancer cell proliferation and metastasis, a deeper mechanistic understanding of IQGAP3 is currently lacking. We have here used TurboID to map IQGAP3 proximity partners and identified the Wnt signaling members Axin1 and CK1α as IQGAP3-interacting proteins. Our functional studies demonstrated that overexpression of IQGAP3 increases β-catenin levels, while IQGAP3 depletion reduces β-catenin levels in gastric cancer cells. Mechanistically, IQGAP3 disrupts Axin1-CK1α interaction, thereby inhibiting β-catenin phosphorylation and ultimately leading to its accumulation. Importantly, we discovered that IQGAP3 itself is regulated by Wnt signaling, suggesting its involvement in a positive feedback loop in Wnt/β-catenin signaling through interactions with Axin1 and CK1α. These findings identify IQGAP3 as a novel mediator of β-catenin stabilization and underscore its potential as a target for cancer therapy.

31 **INTRODUCTION**

32 IQ motif GTPase-activating scaffold proteins (IQGAPs) belong to a family of scaffold proteins,
33 which facilitates physical interactions between effector proteins to coordinate signaling
34 pathways involved in cytoskeleton dynamics (Brandt & Grosse, 2007, Wang, Watanabe et al.,
35 2007), cell proliferation (Nojima, Adachi et al., 2008), and cytokinesis (Adachi, Kawasaki et al.,
36 2014). The mammalian IQGAP family consists of three proteins: IQGAP1, IQGAP2, and IQGAP3.
37 The prevalence of IQGAP1 and IQGAP3 in multiple cancer types indicates fundamental roles in
38 tumorigenesis (Sanchez-Laorden, Viros et al., 2013), indeed, IQGAP1 and 3 have been
39 established as potential targets for cancer therapy (Monteleon, McNeal et al., 2015).
40
41 IQGAP3 is located on chromosome 1q21.3, which is frequently amplified in many malignant
42 tumors (Goh, Feng et al., 2017, Vazquez-Mena, Medina-Martinez et al., 2012). Amongst the
43 IQGAP family, IQGAP3 alone is necessary and sufficient for driving cell proliferation (Nojima et
44 al., 2008). Moreover, *Iqgap3* is specifically expressed in proliferating stomach stem cells and
45 regenerating stomach tissues in the mouse (Matsuo, Douchi et al., 2021). The robust elevation
46 of Iqgap3 following tissue injury is indicative of a requirement for IQGAP3 during wound healing
47 (Matsuo et al., 2021). Injury-induced *Iqgap3* expression is associated upregulation of *Myc* gene
48 targets, embryonic stem cell-like transcriptional signature and importantly, transcriptional
49 programs associated with early gastric cancer (Matsuo, Douchi et al., 2020). More recently, the
50 identification of oncofetal protein IGF2BP1 as a regulator of *IQGAP3* RNA stability suggests that
51 fetal-like reprogramming in tumors led to IQGAP3 overexpression and hyperproliferation of
52 stem-like cancer cells (Myint, Chuang et al., 2022). Mechanistically, IQGAP3 serves as an
53 important hub for multiple oncogenic signaling pathways: PI3K/AKT (Lin, Liu et al., 2019),
54 MAPK/ERK (Nojima et al., 2008, Yang, Zhao et al., 2014) and Wnt/β-catenin (Carmon, Gong et
55 al., 2014). Understanding how IQGAP3 influences these pathways will help the design of
56 effective strategies to inhibit proliferation and promote terminal differentiation in the 'wound
57 that does not heal' – cancer.
58
59 Uncontrolled proliferation is a hallmark of cancer, driven by dysregulated signaling pathways
60 that often involve scaffold and adaptor proteins to ensure precise spatiotemporal coordination.

61 Recent findings highlight the role of biomolecular condensates formed via liquid-liquid phase
62 separation (LLPS) as a key mechanism for coordinating intracellular processes (Mehta & Zhang,
63 2022, Nesterov, Ilyinsky et al., 2021, Tong, Tang et al., 2022), including cancer-related signaling
64 (Hu, Wu et al., 2023, Meng, Yu et al., 2021). Proteins within LLPS function as scaffolds, driving
65 phase separation, or clients, integrating into condensates to enhance multivalent interactions
66 for efficient signal transduction (Banani, Rice et al., 2016). Wnt signaling, crucial for cell
67 proliferation, differentiation, and stem cell maintenance, is frequently dysregulated in cancer,
68 leading to β-catenin stabilization, overexpression of target genes (e.g., *MYC*, *CCND1*, *LGR5*)
69 (Ramakrishnan & Cadigan, 2017), and subsequent tumor growth and metastasis. The β-catenin
70 destruction complex, composed of Axin, APC, GSK3β, and CK1α, regulates β-catenin levels, with
71 Axin's phase separation playing a central role in complex formation and β-catenin
72 phosphorylation. Disruption of Axin polymerization impairs LLPS formation (Bernkopf et al.,
73 2019, Lach, Qiu et al., 2022), promoting Wnt signaling, while β-catenin itself undergoes phase
74 separation via intrinsically disordered regions (IDRs), accumulating at super-enhancers to
75 activate Wnt target genes (Zamudio et al., 2019).
76
77 Our analysis of the IQGAP3 interactome provides an important resource for understanding the
78 role of IQGAP3 in integrating signals from extensive protein networks in cancer. IQGAP3
79 functions as a scaffolding platform, supporting other scaffold proteins in coordinating complex
80 signaling flux from multiple pathways. In this study, we identified Axin1 and CK1α as novel
81 IQGAP3 interaction partner. We demonstrated that IQGAP3 promotes Wnt signaling by
82 stabilizing β-catenin. Mechanistically, IQGAP3 reduces Axin1-CK1α interaction, thereby
83 inhibiting β-catenin phosphorylation on Ser45 and leading to its accumulation. This global
84 increase in β-catenin subsequently promotes the expression of pro-proliferation and survival
85 genes. Finally, we identified an IQGAP3-Wnt feedback loop that sustains Wnt signaling.

RESULTS

Proximity proteomics reveal IQGAP3 interaction with Cdc42, Anillin and with centrosome- and septin-complex proteins

Since both IQGAP3 and Wnt signaling play crucial roles in the maintenance of gastric stem cells and carcinogenesis, we sought to understand the dynamics of IQGAP3 within the Wnt signal transduction network. Given the frequent overexpression of IQGAP3 in various cancer types, we utilized an IQGAP3 overexpression system to study its role in cancer progression. HEK293 cells were chosen for their intact Wnt signaling cascade (i.e., no mutations in Wnt signaling components) (Li, Ng et al., 2012), Wnt-responsiveness (Tuupanen, Turunen et al., 2009) and low basal expression of IQGAP3. We mapped the proximal interactome of IQGAP3 in living cells using the enzyme-catalyzed proximity labeling method, TurboID (Branon, Bosch et al., 2018) with and without Wnt3a stimulation. To induce Wnt signaling, HEK293 Tet-On cells were treated with L-Wnt3a cells (CRL-2647) conditioned media supplemented with rhWnt3a (100 ng/ml) or L-cells (CRL-2648) conditioned media (control) for 4 hours (Fig. 1A). Protein expression and biotinylation levels were validated (Fig. S1A and B) prior to analysis of TurboID-IQGAP3 by label-free quantitative mass spectrometry.

169 and 197 high-confidence IQGAP3 proximity partners were identified in the L-cells conditioned media (-Wnt3a) (Fig. S1C) and L-Wnt3a conditioned media (+Wnt3a) (Fig.S1D), respectively (Fold-change ≥ 4, p value ≤ 0.01), henceforth referred to as -Wnt3a and +Wnt3a treated cells. Amongst these, 100 proximity partners were found in both -Wnt3a and +Wnt3a treated cells (Fig 1B).

To systematically study the interactome profile changes brought about by Wnt3a treatment, we identified shared proximity partners present before and after Wnt3a treatment, exclusive proximity partners before and after Wnt3a treatment, and performed gene ontology analysis to further characterize their compartmentalization, biological and molecular functions.

Consistent with published literature, we observed established interacting partners of IQGAP3, such as Anillin (Adachi et al., 2014) and Cdc42 (Wang et al., 2007) in both interactomes (Fig. 1C). Interestingly, topological analysis of these established partners showed high degree (*k*) within the protein-protein interaction network, indicating their role as hub proteins i.e. proteins that

115 are engaged in essential interactions (Barabasi, Gulbahce et al., 2011, Fox, Hescott et al., 2011,
116 Stelzl, Worm et al., 2005). PCM1, a marker for centriolar satellites (Hori & Toda, 2017) was also
117 identified as a strongly enriched proximity partner of IQGAP3 based on its high rank and degree
118 within the interactomes (Fig. S1C and D).

119 Several complexes were also identified in both interactomes including Septin, CCR4-NOT, HAUS,
120 and myosin complexes. Gene ontology for biological process, molecular function and cellular
121 compartment indicates that the shared proximity partners of -Wnt3a and +Wnt3a treated cells
122 are enriched for Actin Filament organization, Actin binding and Cytoskeleton, in congruence
123 with its role as a regulator of actin cytoskeleton organization (Brandt & Grosse, 2007).

124

125 **Wnt3a treatment promotes IQGAP3 localization to non-membrane organelles and cell**
126 **junctions.**

127 To gain insight into the changes to IQGAP3 proximity partners upon Wnt3a treatment, we
128 compared the proximity partners that were exclusively enriched in the -Wnt3a and +Wnt3a
129 treated cells. Exclusive proximity partners of IQGAP3 in -Wnt3a treated cells (n=69) revealed
130 proteins involved in Wnt signaling; Axin1, APC, PPP2R1A and MACF1 (Fig 2A). Interestingly, all
131 four proteins are scaffold proteins. The presence of IQGAP3 within the proximity of the
132 destruction complex proteins, Axin1 and APC, indicates that it may play a role in Wnt-off
133 condition. In addition, we again observed proteins involved in the CCR4-NOT and HAUS
134 complex, which are known to be involved in mRNA metabolism (Denis & Chen, 2003) and
135 centrosome/spindle integrity (Lawo, Bashkurov et al., 2009), respectively. Lastly, proximity
136 partners found within P-bodies (i.e. dynamic non-membrane bound cytoplasmic structures)
137 such as TOB1, EIF4ENIF1/4E-T, and TNRC6C, may suggest a role for IQGAP3 in the control of
138 translation and mRNA degradation (Decker & Parker, 2012).

139 Meanwhile, exclusive proximity partners of IQGAP3 in +Wnt3a treated cells (n=97) revealed
140 increased in IQGAP3 proximity with cell junction proteins, ESCRT complex, proteins involved in
141 cell division and the centrosome. Notably, we observed the loss of IQGAP3 proximity to Axin1,
142 APC, and MACF1, along with an increased association with β-catenin and enrichment of
143 proteins present in the cell junction, such as Paxillin, Zyxin, and Moesin (Fig. 2B).

144 Next, we compared the Gene ontology for Biological Process enriched in the -Wnt3a and
145 +Wnt3a proximity partners. We observed that -Wnt3a treated cells showed enrichment for
146 proximity partners involved in centrosome cycle, cell membrane projection, microtubule
147 transport, cytoskeleton-dependent cytokinesis, regulation of cytoskeleton and supramolecular
148 fiber organization. Meanwhile +Wnt3a treated cells showed enrichment for proximity partners
149 involved in actin cytoskeleton organization, non-membrane bounded organelle-, organelle- and
150 cell projection-assembly (Fig. 2C).

151 Comparison of the Gene ontology for Cellular Component revealed that -Wnt3a treated cells
152 enriches proximity partners localized to the microtubule cytoskeleton, ruffle, cytoplasm, and
153 centriole. Whereas +Wnt3a treated cells showed enrichment of proximity partners localized to
154 the supramolecular fiber, cell-cell junction, lamellipodium, podosome and actin-based cell
155 projection. Taken together, it appears that IQGAP3 responds to Wnt signaling by first
156 associating with the destruction complex under Wnt-off conditions, and later translocating to
157 the cell junction and actin-based cell projections upon stimulation with Wnt3a.

158 **IQGAP3 undergoes phase separation *in vivo***

159 To visualize changes in IQGAP3 localization within cells, we generated HeLa Tet-On cells stably
160 expressing doxycycline-inducible EGFP-empty (control) or EGFP-IQGAP3 (Fig. 3A). HeLa cells
161 were chosen because they are frequently used in imaging studies. Their large, flat morphology
162 makes them ideal for high-resolution microscopy, as it facilitates the clear visualization of
163 cellular structures, which is critical for protein localization studies.

164 Timelapse experiments revealed the formation of IQGAP3 puncta in both the cytoplasm and
165 nucleus (Fig. 3B and 3C). Furthermore, treatment of EGFP-IQGAP3 cells with Wnt3a resulted in
166 an increased localization of IQGAP3 to the cell junctions, cell projections, and cytoplasmic
167 puncta formation (Fig. 3C). Despite the differences in the cell lines used, these observations
168 were consistent with the interactome data. Next, we treated the cells with 1% 1,6-hexanediol
169 (1,6-HD), an aliphatic alcohol known to disrupt weak hydrophobic interactions and disassemble
170 LLPS-dependent macromolecular condensates with minimal cytotoxicity (Alberti, Gladfelter et
171 al., 2019). As a negative control, the cells were treated with 1% 2,5-Hexanediol (2,5-HD). To
172 track the disruption of the puncta, we performed timelapse imaging before and after 1,6-HD

173 and 2,5-HD treatments. We observed that while treatment with 1,6-HD disrupted EGFP-IQGAP3
174 condensates, treatment with 2,5-HD did not (Fig. 3D). We next examined whether IQGAP3
175 puncta display features distinctive of liquid-like condensates. A key feature of liquid-like
176 condensates is their internal dynamical reorganization and fast exchange kinetics (Hyman,
177 Weber et al., 2014), which can be assessed by measuring the rate of fluorescence recovery
178 after photobleaching (FRAP). We studied the dynamics of EGFP-IQGAP3 condensates by FRAP
179 and observed that EGFP-IQGAP3 displayed dynamic condensate formation distinctive of liquid-
180 like condensates capable of both recovery after bleaching (half time of recovery, $\tau_{1/2}$ = 30.87s)
181 and fusion with other condensates (Fig. 3E and F).

182 **IQGAP3 co-localizes within Axin1 puncta in the cytosol.**

183 Both IQGAP1 and IQGAP3 have been implicated to be involved in Wnt signaling (Carmon et al.,
184 2014). To compare the localization of IQGAP1 and IQGAP3, we overexpressed full length
185 IQGAP1 and IQGAP3 fused to mCherry2 in HeLa cells (Fig. 4B and 4C), and as control mcherry2-
186 empty (Fig. 4A). We counted 50 cells that showed mCherry2-IQGAP1 or mCherry2-IQGAP3
187 expression and categorized them based on the distribution of the IQGAP proteins i.e. when the
188 highest intensity of IQGAP expression is in the membrane, the cell is counted as Mem>Cyto,
189 vice versa (Fig. 4D). We observed that IQGAP1 is predominantly localized to the membrane (Fig.
190 4B) whereas IQGAP3 is localized both in the cytoplasm and nucleus (Fig 4C).

191 Axin1 is a proximity partner of IQGAP3 in the HEK293 interactome. Importantly, Axin1 is known
192 to form LLPS and its puncta formation is correlated with the activity of the β-catenin
193 destruction complex (Bernkopf et al., 2019, Nong et al., 2021, Schaefer & Peifer, 2019, Shi, Kang
194 et al., 2021). To study this phenomenon, we employed the HeLa cell line which is commonly
195 used to model biomolecular condensate formation *in vivo* (Muzzopappa, Hummert et al., 2022,
196 Poudyal, Patel et al., 2023, Shakya, Park et al., 2020). As controls, we expressed mCherry2-
197 empty with EGFP-empty (Fig. 4F-H) and mCherry2-empty with EGFP-Axin1 (Fig. 4I-K). Ectopic
198 expression of EGFP-Axin1 with mCherry2-IQGAP1 (Fig. 4L-N) or mCherry2-IQGAP3 (Fig. 4O-Q)
199 revealed only the colocalization of IQGAP3 within Axin1 puncta. Furthermore, exogenous co-
200 immunoprecipitation of IQGAP1 and IQGAP3 revealed that only IQGAP3 binds Axin1 (Fig. S2A
201 and B). Taken together, the differences in their subcellular distribution may explain the

202 differential binding of IQGAP1 and IQGAP3 to Axin1. Therefore, although both paralogs have
203 been linked to Wnt signaling (Carmon et al., 2014), they likely contribute to distinct aspects of
204 the Wnt signaling cascade.

205 **IQGAP3 expression reduces Axin1-CK1α interaction.**

206 Next, we confirm the endogenous interaction between IQGAP3 and the destruction complex.
207 Endogenous immunoprecipitation of IQGAP3 from HEK293 lysate revealed endogenous IQGAP3
208 interaction with Axin1, β-catenin, CK1α and PCM1 (Fig. 5A). IQGAP3 interaction with Axin1, β-
209 catenin, and CK1α confirms its presence within the destruction complex. IQGAP3 however did
210 not directly interact with other components of the destruction complex; GSK3β and PP2Aα.
211 Similarly, exogenous co-immunoprecipitation experiments involving IQGAP3 with either Axin1,
212 CK1α, GSK3β, PP2Ac, or β-catenin revealed that only Axin1 and CK1α binds to IQGAP3 (Fig. S2B-
213 F), thus indicating the specificity of the interaction.

214 To study the dynamics of IQGAP3-Axin1 interaction, we performed a time-course Wnt3a
215 treatment and performed immunoprecipitation using Axin1 antibody in HEK293T cells
216 overexpressing Myc-IQGAP3 (Fig. 5B). We note that IQGAP3-Axin1 complex formation
217 decreases at 4 hours post Wnt3a treatment due to less Axin1 precipitating as a result of Axin1
218 degradation that occurs at 4 hour post Wnt3a treatment as others have found (Li et al., 2012).
219 This observation explained the loss of Axin1 from the interactome following Wnt3a treatment
220 (Fig. 2B).

221 As expected, Wnt3a treatment showed increased Axin1-β-catenin complex formation with the
222 duration of stimulation (Li et al., 2012). Similarly, immunoprecipitation using IQGAP3 antibody
223 (Fig. 5C) showed increased IQGAP3-β-catenin complex formation with the duration of Wnt3a
224 treatment consistent with the observation that β-catenin interaction is gained in the IQGAP3
225 interactome following Wnt3a treatment (Fig. 2B).

226 To characterize the Axin1-IQGAP3 interaction, we mapped the binding domains and found that
227 IQGAP3 binds to the region between the β-catenin binding domain and the DIX domain (i.e., the
228 CK1α/PP2A binding site) of Axin1 (Fig. 5D) via its IQ and RGCT domains (Fig. S2G-I). Given that
229 IQGAP3 can bind to both CK1α and the CK1α/PP2A binding site within Axin1, we hypothesized
230 that it might disrupt the Axin1-CK1α interaction. Indeed, increased expression of IQGAP3 in

231 HEK293T cells reduced the presence of CK1α in both exogenous Axin1 (Fig. 5E) and endogenous
232 Axin1 (Fig. 5F) precipitates, confirming that IQGAP3 overexpression reduces the Axin1-CK1α
233 interaction. Although we observed that IQGAP3 interacts with Axin1, potentially blocking the
234 Axin1-CK1α interaction, we cannot rule out the possibility that overexpressed IQGAP3 also
235 sequesters CK1α away from Axin1, thereby simultaneously reducing the Axin1-CK1α
236 interaction.

237 **IQGAP3 promotes β-catenin activity through its CC and IQ domains.**

238 We next examined the effect of IQGAP3 overexpression on Wnt signaling. Considering that β-
239 catenin is necessary for Wnt activation and that Axin1 is a critical component of β-catenin
240 destruction complex, we hypothesized that IQGAP3 interferes with β-catenin destruction by
241 reducing the Axin1-CK1α interaction. To test this, we assessed the effects of IQGAP3 depletion
242 and overexpression on exogenous β-catenin in HEK293T cells. Since free excess β-catenin is
243 rapidly phosphorylated by the destruction complex and marked for degradation (Valenta,
244 Hausmann et al., 2012), we used exogenous β-catenin expression to determine whether
245 changes in IQGAP3 could affect this process (Goentoro & Kirschner, 2009).

246 To measure β-catenin activity we perform TOPFlash assay by co-expressing β-catenin with
247 either Axin1 or an increasing amount of IQGAP3. We observed that β-catenin co-expression
248 with Axin1 drastically reduced β-catenin activity, while co-expression with increasing amount of
249 IQGAP3 led to a significant increase in β-catenin activity (Fig. 6A). In contrast, β-catenin co-
250 expression with increasing amount of siIQGAP3 reduced β-catenin activity (Fig. 6B).

251 The priming phosphorylation on Serine 45 of β-catenin is mediated by CK1α and facilitated by
252 Axin1. (Marin, Bustos et al., 2003). Therefore, disruption of Axin1-CK1α interaction will affect
253 S45 phosphorylation and eventually β-catenin levels. Consistent with this, exogenous
254 expressions of IQGAP3 increased non-phosphorylated β-catenin (at Ser45) (hereafter, referred
255 to as ABC), in Wnt-off condition but decreased ABC level in Wnt-on condition (Fig. 6C). Hence,
256 overexpressed IQGAP3 may positively regulate β-catenin activity under Wnt-off conditions;
257 however, it may negatively regulate β-catenin activity under Wnt-on conditions. This dual role
258 of IQGAP3 in Wnt signaling may be explained by the interactome data, which shows that Wnt3a
259 treatment, combined with IQGAP3 overexpression, causes IQGAP3 to relocate to the cell

260 junction with β-catenin. Interestingly, we also observed that Wnt3a treatment increases
261 IQGAP3 expression.

262 To identify the IQGAP3 domain involved in promoting β-catenin activity, we perform TOPFlash
263 assay with a series of IQGAP3 domain deletion constructs (Fig. 6D). Deletion of the Calponin
264 homology domain (ΔCHD), WW domain (ΔWW), GAP-related domain (ΔGRD), and RasGAP C-
265 terminal (ΔRGCT) promoted β-catenin activity (Fig. 6C lanes 3, 5, 7 and 8), whereas deletion of
266 the Coiled coil (ΔCC) and IQ domain (ΔIQ) failed to promote β-catenin activity (Fig. 6D lanes 4
267 and 6). We concluded that both CC and IQ domains are required for promoting β-catenin
268 activity.

269 To gain insight into the function of these domains we amplified the cDNA encoding for the
270 coiled coil (L147 and F669) and IQ (V734 to P849) domains and cloned them into the EGFP-
271 empty vector. We then overexpressed EGFP-coiled coil (CC) and EGFP-IQ in HeLa cells. We
272 observed that EGFP-CC generated distinct puncta formation (Fig. 6G). Similarly, when we
273 studied the dynamics of EGFP-CC condensates using FRAP, we found that EGFP-CC exhibited
274 even higher dynamics in condensate formation after bleaching with a half time of recovery at
275 $\tau_{1/2}$=7.42s compared to EGFP-IQGAP3 at $\tau_{1/2}$=30.87s (Fig. 6G-I). In addition, IQGAP3 deletion of
276 various domains (Fig. S3A-G) showed loss of puncta formation when cell was transfected with
277 the mCherry2-IQGAP3ΔCC construct (Fig. S3C).

278 Meanwhile, cells overexpressed with EGFP-IQ displayed mainly nuclear localization of the
279 peptide (Fig. 6I-K). To confirm that IQ domain is sufficient and necessary for nuclear localization
280 we overexpressed IQGAP3 with an IQ domain deletion (mCherry2-IQGAP3ΔIQ). We observed
281 that IQ deletion abolished any presence of nuclear IQGAP3 (Fig.6L-N) compared to the
282 deletions of other domains (Fig.S3A-G), therefore, the IQ domain within IQGAP3 may harbor a
283 nuclear localization signal (NLS) required for its nuclear localization.

284 Taken together, the CC and IQ domains mediate IQGAP3 phase separation and nuclear
285 localization, respectively. Therefore, it appears that the ability of IQGAP3 to promote β-catenin
286 activity is dependent on its ability to phase separate and translocate to the nucleus.

287 **IQGAP3 overexpression increases β-catenin levels in MKN28 cells.**

288 To determine IQGAP3-low and-high expressing gastric cancer cell lines, we screened several
289 gastric cancer cell lines for the expression of IQGAP3 (Fig. 7A). NUGC3 and AGS cells showed
290 high IQGAP3 expression, whereas MKN28 cells showed low IQGAP3 expression, hence, the
291 latter was deemed a suitable candidate to study the effect of IQGAP3 overexpression in gastric
292 cancer cells. MKN28 cells stably overexpressing doxycycline-inducible 3×Flag-IQGAP3 when
293 treated with doxycycline showed increased β-catenin levels (Fig. 7B).

294 Furthermore, the RNA-seq analysis from IQGAP3 overexpressing cells, revealed an enrichment
295 for several signaling pathways, G2/M, TGF-β, NOTCH, and Wnt/β-catenin in the GSEA data (Fig.
296 7C). Similarly, the gene ontology analysis of the Biological Process (GO) revealed enrichment in
297 the Wnt signaling pathway (Fig. 7D), the Molecular Function (GO) showed enrichment in Wnt-
298 protein and beta-catenin binding (Fig. 7E), and the KEGG pathway analysis indicated
299 enrichment in the Wnt signaling pathway (Fig. 7F).

300 Lastly, proximity ligation of IQGAP3 within MKN28 cells revealed Axin1 as a proximity partner of
301 IQGAP3. The presence of IQGAP3 in proximity to Axin1 in both HEK293 and MKN28 cells
302 strongly suggests its involvement in the destruction complex (Fig 7G). Induction of fusion
303 protein expressions and biotinylating activities were analyzed by immunoblot (Fig. S4A and S4B).
304 MKN28 interactome mapping, volcano plot and full list of GSEA ranking from RNA-sequencing
305 analysis (Fig. S4C-E).

306

307 **IQGAP3 knock-out decreases β-catenin levels in NUGC3 and AGS cells.**

308 The canonical Wnt pathway is best known for its regulation of cell proliferation (Jung & Park,
309 2020). We next ascertained how IQGAP3 status affects Wnt-driven proliferative potential, we
310 performed CRISPR-mediated IQGAP3 knock-out in two gastric cancer cell lines: the *TP53* mutant
311 NUGC3 and the constitutively active Tcf transcriptional activity (CTTA) AGS cell line (Caca,
312 Kolligs et al., 1999). As screened previously, both cell lines exhibit high IQGAP3 expression (Fig.
313 7A), making them suitable candidates for CRISPR-mediated knock-out.

314 IQGAP3-KO NUGC3 cells showed reduced total β-catenin levels (Fig. 8A) and decreased
315 expression of Wnt target genes (*CCND1* and *MYC*) (Fig. 8B) compared to NUGC3 wild-type cells.
316 Moreover, both cell proliferation (Fig. 8C) and clonogenic growth (Fig. 8D and E) were also
317 impaired.

318 Relevant to Wnt signaling, AGS harbor mutations for the following proteins; *CTNNB1* (G34E)
319 (Caca et al., 1999) and *CDH1 (*G579fs) (Caldeira, Figueiredo et al., 2015). These mutations result
320 in the accumulation of β-catenin and loss of E-cadherin expression, respectively. Loss of IQGAP3
321 impaired cell proliferation and clonogenic growth in the AGS gastric cancer cell line (Fig. 8H-J).
322 Importantly, AGS IQGAP3 knock-out (IQ3KO) displayed significant loss of β-catenin relative to
323 the AGS parental counterpart (Fig. 8F). Concomitantly, the expression of Wnt target genes
324 involved in promoting proliferation and cell-cycle re-entry, *CCND1* and *Myc* (Niehrs & Acebron,
325 2012, Nusse, 2008, van de Wetering, Sancho et al., 2002) were also reduced in AGS IQ3KO cells
326 (Fig. 8G).

327 In line with our findings, the relationship between IQGAP3 expression and β-catenin levels has
328 also been previously observed, whereby the loss of IQGAP3 expression via siRNA-mediated
329 knockdown in pancreatic cancer cell lines BxPC-3 and SW1990 have been shown to reduce β-
330 catenin expression (Xu, Xu et al., 2016). Hence, our observation that the loss of IQGAP3
331 reduces β-catenin expression in gastric cancer cells may also apply to other cancer types.

332

333 **IQGAP3 is a target of Wnt signaling, sustains Wnt signaling via positive feedback loop.**

334 Wnt activity in epithelial stem cells are tightly regulated. Wnt-signaling levels below a specific
335 threshold can be lethal due to the rapid turnover rate of the epithelium, as observed in mouse
336 models of Tcf4 conditional knock-out (van Es, Haegebarth et al., 2012) or DKK overexpression
337 (Kuhnert, Davis et al., 2004). Conversely, excessively high Wnt-signaling resulted in the
338 overproduction of crypts, the formation of adenomas, and the development of cancer (Polakis,
339 2012). To maintain stringent control, the pathway incorporates various molecular checkpoints
340 and feedback loops, where pathway components (e.g. AXIN2 (Leung, Kolligs et al., 2002), DKK1
341 (Niida, Hiroko et al., 2004), SFRP1 (Caldwell, Jones et al., 2006), WIF1 (He, Reguart et al., 2005),

342 CD44 (Schmitt, Metzger et al., 2015), and NKD1 (Van Raay, Coffey et al., 2007)) play distinct
343 regulatory roles.
344
345 To assess whether IQGAP3 is involved in the Wnt feedback loop, we treated HEK293T cells with
346 Wnt3a conditioned media and analyzed IQGAP3 transcript and protein expression. As expected,
347 RT-qPCR revealed increased expression of known Wnt targets, including AXIN2, CCND1, MYC,
348 LEF1, TCF7, and TCF7L2 (also known as TCF4), following Wnt3a conditioned media treatment.
349 Interestingly, we also observed a Wnt3a-associated increase in IQGAP3 transcript levels (Fig.
350 9A). Supporting this, a time-course analysis of Wnt3a conditioned media treatment in HEK293T
351 cells showed elevated IQGAP3 expression over time (Fig. 9B). Additionally, probing for IQGAP3
352 expression in L cells and L-Wnt3a cells revealed higher IQGAP3 levels in L-Wnt3a cells compared
353 to L cells (Fig. S3H). Together, these findings strongly suggest that IQGAP3 is a Wnt target gene.
354
355 We next investigated how Wnt signaling regulates *IQGAP3* transcription. The Genome browser
356 revealed multiple canonical TCF4 binding motifs (A/T-A/T-C-A-A-A-G or C-T-T-T-G-A/T-A/T) (van
357 de Wetering & Clevers, 1992) within the *IQGAP3* promoter (*IQGAP3*P). The promoter region of
358 *IQGAP3* spanning 4320bp (-3000 to +1320bp of TSS), a series of *IQGAP3*P 5'-truncations, and
359 *Axin2* promoter *(Axin2*P) spanning 1730bp (-581 to +1149bp of TSS) were cloned into the pGL3-
360 basic firefly luciferase reporter vector. We observed that both the full length *IQGAP3*P (-3000 to
361 +1320 of TSS) and *Axin2*P responded to Wnt3a treatment, while the truncated *IQGAP3*P
362 constructs did not (Fig. 9D). Thus, we hypothesized that a Wnt Responsive Element (WRE)
363 might reside within -3000 to -2000bp of the TSS. Indeed, a truncation comprising the smaller
364 fragment of -3000 to -2000bp (Site 1) displayed strong luciferase activity upon Wnt3a-CM
365 treatment, similar to *Axin2*P, whereas negative control Site 2 (+335 to +1265 of the TSS) did not
366 (Fig. 9E). Within Site1 we identified two potential WREs located within -2815 to -2808bp and -
367 2810 to -2803bp of the TSS, harboring the motifs CTTTGAA and CTTTGTA, respectively. Next, we
368 mutated the motifs: CTTTG<u>AA</u> to CTTTG<u>GC</u> (Site1aM) and CTTTG<u>TA</u> to CTTTG<u>GC</u> (Site1bM) and
369 observed that both Site1a and Site1b are necessary for Wnt3a-mediated upregulation of
370 IQGAP3 transcription (Fig.9F). Taken together, our findings confirm that IQGAP3 is a Wnt target.
371

372 **DISCUSSION**

373 Scaffold protein IQGAP3 is upregulated in most, if not all, cancer cells and has been shown to be
374 required for proliferation (Nojima et al., 2008). Identifying the IQGAP3 interactome in cancer
375 cells is thus a critical step to develop anti-IQGAP3 therapeutics in cancer. Traditional
376 immunoprecipitation/mass spectrometry techniques may miss transient, but crucial
377 interactions in the IQGAP3 scaffold function. Here, we utilize Proximity ligation labelling to
378 systemically characterize the molecular interactions and mechanisms underlying the IQGAP3
379 scaffold function in cancer.

380 We identified large networks of IQGAP3 interacting proteins in the cell cycle as well as
381 oncogenic pathways. Based on our interactome data, IQGAP3 is associated with different
382 protein complexes located at various locations of the cell and phases of the cell cycle. We
383 observed that IQGAP3 proximity partners were enriched for proteins found in non-membrane
384 bounded organelle or phase separated microenvironment. By forming interactions with other
385 phase-separated scaffold proteins, IQGAP3 could penetrate the specialized microenvironments
386 of various biochemical reactions and thus regulate these reactions.

387 In this study, we have uncovered a previously unknown function of IQGAP3. IQGAP3 expression
388 disrupts Axin1-CK1α interaction, either by blocking CK1α binding to Axin1, sequestering CK1α
389 away from Axin1, or both, thereby inhibiting β-catenin phosphorylation and promoting its
390 stabilization (Fig 10). Notably, we identified that the coiled-coil (CC) domain of IQGAP3 is
391 essential for its phase separation, while the IQ domain is necessary for its nuclear localization.
392 Both functions are critical for IQGAP3 to enhance β-catenin activity. This dependence on the
393 coiled-coil domain to phase separate resembles proteins such as, Amot (Wang, Choi et al., 2022,
394 Wells, Fawcett et al., 2006), KIBRA (Wang et al., 2022), SLMAP (Wang et al., 2022), TAZ (Lu, Wu
395 et al., 2020), YAP (Mao, Liu et al., 2023), liprin-α (Liang, Jin et al., 2021), LINE-1 ORF (Newton,
396 Naik et al., 2021), and RNA-Binding Proteins (RBPs) (Ford & Fioriti, 2020). In addition, the IQ
397 domain potentially harbors the nuclear localization sequence (NLS), similar to what others have
398 observed for IQ-domain containing proteins (Dzijak, Yildirim et al., 2012, Fischer, Kugler et al.,
399 2013).

400 In addition, we observed that Wnt3a treatment promotes IQGAP3 expression both at the
401 transcript and protein levels. Wnt signaling is tightly regulated with multiple feedback loops,
402 where most Wnt regulators are themselves Wnt target genes (Zhong & Virshup, 2020). Similarly,
403 IQGAP3 is both a regulator and target of Wnt signaling. This Wnt-associated function of IQGAP3
404 supports previous findings that implicate IQGAP3 in promotion of cancer proliferation and stem
405 cell regeneration. Therefore, targeting IQGAP3 during early stages of cancer could potentially
406 help mitigate both the growth and spread of cancers.

407

408 **MATERIALS AND METHODS**

409

410 **Cell culture, transfection and conditioned media**

411 HEK293T (CRL-3216), L-Cells (CRL-2648), and L-Wnt3a cells (CRL-2647) were from ATCC. HEK293
412 Tet-On® 3G Cell Line #631182 was from Takara bio. Immortalized human normal gastric
413 epithelial cells (HFE145) were obtained from Dr. Hassan Ashktorab and Dr. Duane Smoot. Both
414 HEK293 and HEK293T cells were cultured in Dulbecco's modified Eagle's medium (DMEM) while
415 the gastric cancer cell lines, AGS, MKN1, MKN28, HFE145 and NUGC3 cells were cultured in
416 RPMI-1640, both growth media were supplemented with 10% fetal bovine serum (FBS) and 1%
417 Penicillin-Streptomycin solution. The Dox-inducible 3×HA-TurboID-empty and 3×HA-TurboID-
418 IQGAP3 expressing cells were generated by transfection of pRetroX-3×HA-TurboID-empty or
419 pRetroX-3×HA-TurboID-IQGAP3 in the HEK293-Tet-On and MKN28-Tet-On cells, thereafter,
420 stable population were selected with 1.0 µg/ml Puromycin.

421 All Dox-inducible TurboID stable expressing cells were cultured and maintained in DMEM
422 supplemented with 10% fetal bovine serum (FBS), 0.5 µg/ml Puromycin (Gibco), 1 µg/ml
423 Doxycycline (Sigma), 200 µg/ml Geneticin (Gibco). Transfections were carried out using
424 Lipofectamine 2000 (Thermofisher) according to the manufacturer's instructions. CRISPR knock-
425 out cells were cultured and maintained in RPMI supplemented with 10% fetal bovine serum
426 (FBS), and 0.5 µg/ml Puromycin. Conditioned media from L-cells and L-Wnt3a cells were
427 harvested 72-96 hours after cell seeding and filtered through 0.45 µm syringe filter and stored
428 in -80°C. All Wnt3a conditioned media were supplemented with 100 ng/ml rhWnt3a #5036-WN
429 (RnDSystems).

430

431 **Antibodies and Plasmids**

432 Antibodies specific for the following proteins were used at the indicated dilutions for
433 Immunoblot: α-Tubulin 11224-1-AP (1:10,000, Proteintech®); IQGAP3 #25930-1-AP, mCherry
434 #26765-1-AP (all 1:1000, Proteintech®); Flag M2 #F1804 (1:1000, Sigma); Axin1 #2087, β-
435 catenin #8480, Non-phospho (Active) β-Catenin (Ser45) #19807, Non-phospho (Active) β-
436 Catenin (Ser33/37/Thr41) #8814, Myc-Tag #2276, HA-Tag #3724 & #2367, GSK-3β #12456,

437 PP2A C #2038 (all 1:1000, Cell Signaling). Streptavidin-HRP #ab7403 (1:40,000, Abcam); IQGAP1
438 #ab86064 (1:1000, Abcam), CK1α Antibody (H-7): sc-74582 (1:250, Santa Cruz).

439 Antibodies specific for the following proteins were used at the indicated dilutions for
440 immunoprecipitation: Axin1 #2087 (1:100, Cell Signaling), Myc-Tag (9B11) #2276 (1:100, Cell
441 Signaling). Anti-Flag® M2 #F1804 (1:100 Sigma), IQGAP3 (H00128239PW2) #89-301-822 (1:100,
442 Abnova).

443 The following plasmid was obtained from Vectorbuilder:

444 pCMV-EGFP-IQGAP3

445 The following plasmids were obtained from Addgene:

446 3xHA-TurboID pRetrox (from Kyle Roux, #155203), pGL3-OT and pGL3-OF (from Bert Vogelstein,
447 #16558 & #16559), Flag-Axin1 (from Mariann Bienz, #109370), β-catenin-Flag (from Eric Fearon,
448 #16828), LentiCRISPRv2 (from Feng Zheng, #52961), pMD2.G and psPAX2 (from Didier Trono
449 #12259 and #12260), mCherry2-C1 (from Michael Davidson, #54563), pcDNA3-EGFP-empty
450 (Doug Golenbock, #13031), pcDNA3-GSK3β-HA (from Jim Woodgett, # 14753), pLC-Flag-
451 CSNK1A1 WT-Puro (from Eva Gottwein #123319)

452

453 **Molecular cloning**

454 Cloning was performed using either In-Fusion HD Cloning Kits (Takara) via Ligation Independent
455 Cloning (LIC) or Restriction cloning using enzymes purchased from New England Biolabs (NEB).

456 Full-length IQGAP3 coding sequence was cloned from pCMV-IQGAP3-GFP and inserted into
457 3xHA-TurboID pRetrox, pcDNA3-Flag-empty, pcDNA3-Myc-empty, and mCherry2-C1. Full-length
458 Axin1 coding sequence was cloned from Flag-Axin1 and inserted into pcDNA3-EGFP-empty and
459 pcDNA3-HA-empty. Full-length β-catenin coding sequence was cloned from β-catenin-Flag and
460 inserted into pcDNA3-HA-empty. Full-length CK1α coding sequence was cloned from pLC-Flag-
461 CSNK1A1 WT-Puro and inserted into pcDNA3-HA-empty.

462 cDNA expressing EGFP-CC was amplified from the pCMV-EGFP-IQGAP3 vector using the
463 following primers: EcoRI-CC-For, TAAGCAGAATTCCTCTTCCTCTTCCGGCTGGG and XhoI-CC-Rev,

464 TGCTTACTCGAGGAAAGCTGTGTCTGCTGG generating a 1593 bp primer product that was later
465 cloned into an EGFP-vector backbone. Similarly, EGFP-IQ was amplified from pCMV-EGFP-
466 IQGAP3 vector using the following primers: EcoRI-IQ-For,
467 TAAGCAGAATTCGTTATCCAGCTCCAGGCCCG and XhoI-IQ-Rev,
468 TGCTTACTCGAGCTAAGGGTGGGGTGCATGCAC generating a 375 bp primer product that was
469 later cloned into an EGFP-vector backbone.

470

471 **Promoter cloning**

472 Promoter sequences of *AXIN2* and *IQGAP3* were obtained from Ensembl. *IQGAP3* promoter
473 (*IQGAP3P*): A region spanning 4320bp located on chr1: 156,571,285-156,575,604
474 (GRCh38/hg38) or chr1:156,541,077-156,545,396 (GRCh37/hg19) and *AXIN2* promoter
475 (*AXIN2P*): A region spanning 1730bp located on chr17: 65,560,500-65,562,229 (GRCh38/hg38)
476 or chr17:63,556,618-63,558,347 (GRCh37/hg19). Both promoter sequences were PCR amplified
477 using genomic DNA isolated from HEK293T cells with KAPA HiFi PCR Kit. Primer-BLAST was used
478 to verify the specificity of primer design. In-Fusion HD Cloning Kits (Takara) were used in
479 Ligation Independent Cloning (LIC) of PCR product into pGL3 basic vector. Primer sequences
480 excluding homology sequences (added for LIC) are as follows, for *IQGAP3P* forward primer: 5'-
481 ACCTATAGATGTAACTTGTCCAAG-'3 and reverse primer: 5'-GTAAGAAAATAAACTCAGAGAGCTT-
482 3', for *AXIN2P* forward primer: 5'-CACTCAGGCCTATACTGGCG-3' and reverse primer: 5'-
483 CACGCCGACTCACATCCATA-3'. All promoter plasmid constructs were co-transfected with pSV-β-
484 Galactosidase (internal control) into HEK293T cells with and without Wnt3a-CM treatment to
485 validate the putative Wnt responsive element (WRE) within the promoter region.

486

487 **gRNA design and plasmids**

488 The sgRNA sequence including PAM region targeting exon 5 of *IQGAP3* was determined using
489 IDT (sg.idtdna.com/site/order/designtool/index/CRISPR_SEQUENCE) as follows; 5'-
490 TGGATGCAGTAGACTACCCG GGG-3'. While sgRNA targeting exon 17 of *IQGAP3* was determined
491 using CRISPR Design Tool (www.genscript.com/CRISPR-gRNA-constructs.html) as follows; 5'-

492 GTCGGGAACTACCCCTCGAA GGG-3'. sgRNA oligos were cloned into LentiCRISPRv2 plasmid
493 (Addgene #52961) at BsmBI restriction sites (Sanjana, Shalem et al., 2014).

494

495 **Lentiviral vector construction and transduction**

496 Lentiviral vectors were produced by co-transfecting HEK293T cells with the transfer plasmid
497 sgRNA-Cas9-expressing lentiCRISPRv2, the packaging plasmid pMD2.G and psPAX2 using
498 Lipofectamine 2000 transfection reagent. Briefly, for each sgRNA, a plate of 10-cm plate of 60%
499 confluent 293T cells was transfected with 10 µg of the transfer plasmid, 5µg of pMD2.G, 7.5µg
500 of psPAX2, and 40 ul of Lipofectamine 2000 (Life Technologies). After 24 hours, the media was
501 replaced with fresh media. After 48 hours, viral supernatants were collected and centrifuged at
502 3,000 rpm at 4 °C for 5 min to pellet cell debris. The supernatant was filtered through a 0.45 µm
503 low protein binding membrane (Millipore) and used immediately after supplementing with
504 7µg/ml of polybrene or stored in -80°C. Successful knock-out colonies were selected with
505 Puromycin treatment, 1 µg /ml.

506

507 **Immunoblot**

508 Cells were lysed with RIPA lysis buffer (ThermoSci) supplemented with Protease inhibitor
509 cocktail (Roche) and Halt™ Phosphatase Inhibitor Cocktail (Thermo Scientific™). For all unless
510 specified, 20 µg of total protein from each sample were subjected to 7.5% or 10% SDS
511 polyacrylamide gel electrophoresis (PAGE) and electrophoretic transfer onto 0.2 µm
512 polyvinylidene difluoride (PVDF) membrane (Bio-Rad) at 30 V, 100 mA, 4 °C overnight. The
513 transfer buffer (Towbin) comprises 25 mM Tris, 192 mM glycine, 20% (v/v) methanol, pH 8.3.
514 Membranes were incubated with primary antibodies in either 0.5% BSA or skimmed milk in
515 TBST (Tris Buffered Saline + 0.1% (v/v) Tween 20) overnight, following which were washed 3
516 times with TBST and incubated with secondary antibody conjugated with HRP (1:5000) in 0.5%
517 BSA or skimmed milk in TBST for 1 hour at room temperature. Membranes were then washed 3
518 times with TBST. Antibody detection was performed using Radiance plus chemiluminescent
519 substrate (azure biosystems). Antibody reactions detection was imaged using ImageQuant LAS

520 500 (GE Healthcare). When re-probing with a different primary antibody, membranes were
521 stripped using Mild stripping buffer pH 2.2 (1.5% (w/v) Glycine, 1% (w/v) SDS, and 1% Tween 20)
522 in room temperature for 10 minutes and thereafter washed with TBS for 10 minutes twice and
523 with TBST for 10 minutes twice. Uncropped images of all immunoblots can be found in the
524 supplementary image file.

525

526 **Immunofluorescence staining**

527 Cells were fixed with 4% paraformaldehyde for 30 minutes and washed with PBS three times
528 for 5 minutes each. Cells were then permeabilized with PBS containing 0.1% Triton X-100 for 10
529 minutes. Permeabilized cells were then incubated in blocking buffer (0.5% BSA/0.1% Triton X-
530 100) for 1 hour, and following that with the appropriate primary antibody diluted in antibody
531 dilution buffer (0.5% BSA/0.3% Triton X-100) overnight in 4˚C. After three washes with PBS for 5
532 minutes each, cells were incubated with Alexa Fluor 488- or 594-conjugated secondary
533 antibodies (1:100 dilution) for 1 hour. Cells were then washed with PBS three times for 5
534 minutes each and mounted with DAPI. Fluorescence was observed under Zeiss LSM 880 Airy
535 Scan.

536

537 **Live Cell Imaging**

538 HeLa Tet-On cells stably expressing Doxycycline inducible EGFP-empty and EGFP-IQGAP3 were
539 seeded onto a 35 mm cell imaging dish with a glass bottom (Matsunami). Cells were induced
540 with Doxycycline 24-48 hours prior to live imaging.

541

542

543 **Fluorescence recovery after photobleaching (FRAP)**

544 HeLa cells grown on Glass Bottom Culture Dishes (Matsunami Glass) were transfected with 2 µg
545 per well of GFP–CC and analyzed through quantitative FRAP studies 24h after transfection.
546 FRAP experiments were performed using a Zeiss LSM880 confocal microscope. The

547 fluorescence signal was bleached using 100% of maximum laser power of the 488-nm laser with
548 150 interactions for ~2.5 s. Relative recovery was normalized to the initial (before bleaching)
549 fluorescence intensity for each bleached condensate and then used to calculate mean and SD of
550 the recovery time. To compare the post-bleach recovery 5 pre-bleach images were captured.

551 For the treatment of 1,6-hexanediol (1,6-HD), culture media was replaced with 5% 1,6 HD
552 prepared in DMEM culture media, which was replaced with fresh culture media to monitor the
553 recovery after 1,6 HD treatment. Apart from the bleached region, fluorescence intensity mean
554 was also recorded for non-bleached and background. Raw FRAP data was further analyzed
555 using easyFRAP online analysis tool (Koulouras et al., 2018). All acquired images were processed
556 and analyzed in ImageJ software.

557

558 **Co-immunoprecipitation**

559 Cells were lysed with immunoprecipitation lysis buffer (IPLB) containing 25 mM Tris pH 7.5, 150
560 mM NaCl, 0.5% Triton-X, protease inhibitor cocktail (Roche) and Halt™ Phosphatase Inhibitor
561 Cocktail (Thermo Scientific™). For Flag-tagged and endogenous protein immunoprecipitation,
562 cell lysates were incubated with Protein G magnetic beads (Millipore) for 2 hours (pre-clearing).
563 The beads were removed, and primary antibody was then added to protein lysates at a
564 concentration of 1:100 and incubated overnight at 4°C. 15 µl of Protein G magnetic beads
565 (Millipore) is then added to the Protein-Antibody complex and incubated at 4°C for 2 hours. The
566 Protein G magnetic beads (Millipore) were then washed with IPLB three times and protein
567 complex were eluted by adding SDS sample buffer and boiling for 5 minutes.

568

569 **Biotin pulldowns**

570 Using the TurboID method (Branon et al., 2018), proteins in close proximity to IQGAP3 were
571 biotinylated and isolated by streptavidin-bead pulldowns. Briefly, 24 hr after Dox induction and
572 biotin supplementation (50 µM), biotinylated proteins were enriched from the protein extracts
573 with 50 µL of streptavidin-coated magnetic beads (Dynabeads™ MyOne™ Streptavidin C1,
574 Invitrogen, #65001). Beads were washed twice with RIPA lysis buffer, the lysates containing

575 2 mg protein were then incubated with the equilibrated beads on a rotator overnight at 4 °C.
576 The beads were washed twice each with wash buffer 1 (2% SDS), wash buffer 2 (50 mM Hepes
577 pH 7.5, 500 mM NaCl, 1 mM EDTA, 1% Triton-X-100, 0.5% Na-deoxycholate), wash buffer 3 (10
578 mM Tris pH 8, 250 mM LiCl, 1 mM EDTA, 0.5% NP-40, 0.5% Na-deoxycholate) and wash buffer 4
579 (50 mM Tris pH 7.5, 50 mM NaCl, 0.1% NP-40). Biotinylated proteins were eluted by boiling the
580 beads in 35 µL of 1 × Laemmli sample buffer. Eluted proteins were sent for Mass spectrometry
581 analysis.

582

583 **Mass spectrometry analysis**

584 TurboID samples were separated on a 4-12% NuPAGE Bis-Tris precast gel (Thermo Fisher
585 Scientific) for 10 min at 170 V in 1x MOPS buffer. The gel was fixed using the Colloidal Blue
586 Staining Kit (Thermo Fisher Scientific) and processed as a single fraction. For in-gel digestion,
587 samples were destained in destaining buffer (25 mM ammonium bicarbonate; 50% ethanol),
588 reduced in 10 mM DTT for 1h at 56°C followed by alkylation with 55mM iodoacetamide (Sigma)
589 for 45 min in the dark. Tryptic digest was performed in 50 mM ammonium bicarbonate buffer
590 with 2 µg trypsin (Promega) at 37°C overnight. Peptides were desalted on StageTips and
591 analysed by nanoflow liquid chromatography on an EASY-nLC 1200 system coupled to a Q
592 Exactive HF mass spectrometer (Thermo Fisher Scientific). Peptides were separated on a C18-
593 reversed phase column (25 cm long, 75 µm inner diameter) packed in-house with ReproSil-Pur
594 C18-AQ 1.9 µm resin (Dr Maisch). The column was mounted on an Easy Flex Nano Source and
595 temperature controlled by a column oven (Sonation) at 40°C. A 105-min gradient from 2 to 40%
596 solution B (80% acetonitrile, 0.1% formic acid) at a flow of 225 nl/min was used. Spray voltage
597 was set to 2.2 kV. The Q Exactive HF was operated with a TOP20 MS/MS spectra acquisition
598 method per MS full scan. MS scans were conducted with 60,000 at a maximum injection time of
599 20 ms and MS/MS scans with 15,000 resolution at a maximum injection time of 75 ms. The raw
600 files were processed with MaxQuant version 2.0.1.0 (HEK293) and 1.5.2.8. (MKN28) with preset
601 standard settings for label-free quantitation using the MaxLFQ algorithm.
602 Carbamidomethylation was set as fixed modification while methionine oxidation and protein N-
603 acetylation were considered as variable modifications. Search results were filtered with a false
604 discovery rate of 0.01. Known contaminants, proteins groups only identified by site, and reverse

605 hits of the MaxQuant results were removed and only proteins with LFQ intensities in four
606 replicates of at least one condition of each pair-wise comparison were kept. Missing LFQ
607 intensities were randomly inputed from a normal distribution around the lowest 5% of LFQ
608 intensities based on the means of three iterations.

609

610 **Cell viability assay**

611 Cell viability was determined using the TACS® XTT Cell Proliferation Assay (R&D Systems, Inc.),
612 following the manufacturer's instructions. Gastric cancer cell lines NUGC3 and AGS along with
613 their corresponding IQGAP3KOs were seeded at 1×10^3 cells/mL density in 100 µL of
614 appropriate growth medium in 96-well microplates. After incubation overnight, to allow cell
615 attachment, which was considered as 0H and analyzed, followed by analysis after time periods
616 of 24, 48, 72 and 96 hours. For analysis, 50 µL of XTT Working Solution (prepared by combining
617 XTT Reagent and XTT Activator as per kit instructions) were added to each well. Plates were
618 incubated for 6 hours at 37°C in a 5% CO_2 atmosphere. The absorbance was measured at 490
619 nm (test wavelength) with a reference wavelength of 630-690 nm using a microplate reader.

620

621 **Clonogenic Assay**

622 Gastric cancer cell lines NUGC3 and AGS along with their corresponding IQGAP3KOs were
623 seeded in 6-well plates at a density of 500 cells per well in 2 mL of complete growth medium
624 and incubated at 37°C in 5% CO_2. The cells were grown with necessary media change when
625 required for 7–14 days to allow colony formation. At the end of the incubation period, the
626 medium was removed, and cells were gently rinsed with PBS. Colonies were fixed and stained
627 with a mixture of 6.0% glutaraldehyde and 0.5% crystal violet for 30 minutes. The staining
628 solution was removed, and plates were rinsed in tap water and air-dried at room temperature.
629 Colonies consisting of ≥50 cells were counted manually under a light microscope. The colony-
630 forming efficiency (CFE) was calculated as: CFE (%) = Colonies formed / Cells seeded×100

631

632 **Luciferase assay**

633 5×10^4 HEK293T cells were grown per well in a 24-well plate for 24 hours, thereafter cells were
634 transfected with the appropriate plasmids: for TOPFLash (TCF wild-type (OT) or TCF mutant (OF)
635 plasmids); for promoter analysis (*IQ3P* or *Axin2P*), together with pSV-β-Galactosidase vector as
636 control vector for monitoring the transfection efficiency. Cells were grown for an additional 48-
637 hours before lysis. If Wnt3a conditioned media were used, cells were exposed to the
638 conditioned media 24-hours before lysis. Lysis was performed using 5×Passive lysis buffer
639 (Promega, #E1910), lysates were rocked in room temperature for 15 mins. Thereafter, lysates
640 were centrifuged for 10 mins at 14,000 rpm to remove cell debris. Lysate supernatants used
641 were aliquoted into white, flat bottom, 96-well plate (Costar) for treatment with either Beta-
642 Glo® (Promega, #E4720) or Luciferase Assay Reagent II/LARII (Promega, #E1910) reagent.

643

644 **Real-Time Polymerase chain reaction (RT-PCR)**

645 RNA extraction was performed using RNeasy Mini Kit (Qiagen). 1 µg of Purified RNA was reverse
646 transcribed to complementary DNA (cDNA) using iScript™ Reverse Transcription Supermix (Bio-
647 Rad). cDNA was diluted 10×. RT-PCR was performed on QuantStudio™ 3 Real-Time PCR System
648 (Applied Biosystems). The 20 µl PCR reaction mixture consisted of 2 µl of cDNA, 100 nM
649 forward and reverse primers, 2× iTaq Universal SYBR Green Supermix. Cycling conditions were
650 initial denaturation at 95 °C for 5 minutes, followed by 40 cycles consisting of 95 °C for 10
651 seconds, 60 °C for 30 seconds and 72 °C for 10 seconds.

652 The primers used for real-time RT-PCR were as follows:

Genes	**Forward** (5'-3')	**Reverse** (5'-3')
AXIN2	AGCTTACATGAGTAATGGGG	AATTCCATCTACACTGCTGTC
CCND1	TCTACACCGACAACTCCATCCG	TCTGGCATTTTGGAGAGGAGGTG
MYC	CTTCTCTCCGTCCTCGGATTCT	GAAGGTGATCCAGACTCTGACCTT
LEF1	GGTCCTCCTGGTCCCCACACAA	TCATGCTGAGGCTTCACGTGCA
TCF7	CTGACCTCTCTGGCTTCTACTC	CAGAACCTAGCATCAAGGATGGG
TCF7L2	GAATCGTCCCAGAGTGATGTCG	TGCACTCAGCTACGACCTTTGC
IQGAP3	GTTCGGCAGAAGTTTGCTGAGC	CACTCCAGGTAAATCTTCCGCTG
GAPDH	TCTTTTGCGTCGCCAGCCGA	ACCAGGCGCCCAATACGACC

653

654 **Fluorescence Intensity Analysis**

655 To determine mCherry2 intensity for localization of IQGAP1 and IQGAP3. The cross-sectional
656 line was drawn in ImageJ. Lines were fixed by the ROI manager to ensure a similar length for
657 image comparison. Lines were then analyzed using Plot Profile.

658

659 **Co-localization Analysis**

660 To determine mCherry2/EGFP co-localization, channels were split in ImageJ and the JACoP
661 plugin was used. The Pearson's Coefficient generated from 50 cells were averaged.

662

663 **General Statistical Analysis**

664 Experimental data are presented as the mean ± SD. Two-tailed Student's t tests with unequal
665 variance were performed using XLMiner Analysis ToolPak on Microsoft excel.
666 Error bars represent standard deviation. Differences were considered statistically significant
667 when p values were less than 0.05 ($^{*}p < 0.05$, $^{**}p < 0.01$, $^{***}p < 0.001$). The best represented
668 images were shown.

669

670 **Author contributions**

671 M.B.R. conceptualized the study. M.B.R. and Y.I. analyzed the data. A.H. performed XTT and
672 Clonogenic assays. D.K. and S.P. performed the mass spectrometry analysis. M.B.R. and T.Y.X.
673 performed the confocal imaging. M.B.R and B.D. performed the FRAP analysis. M.B.R. created
674 the Tet-On and CRISPR-KO cells. M.B.R. and Y.I. wrote the manuscript.

675

676 **ACKNOWLEDGEMENTS**

677 We thank Dr. Hassan Ashktorab and Dr. Duane Smoot for the Immortalized human normal
678 gastric epithelial cells (HFE145).

679 This research was supported by grants from the National Research Foundation Singapore and
680 the Singapore Ministry of Education under its Research Centers of Excellence initiative, the
681 Singapore Ministry of Health's National Medical Research Council under its Clinician-Scientist
682 Individual Research Grant (MOH-000933-00) and the National Medical Research Council's Open
683 Fund Large Collaborative Grant (OFLCG18May-0023), National University of Singapore School of
684 Medicine (NUSMed) Internal Grant Funding (NUHSRO/2019/086/ StomachStemCell and
685 NUHSRO/2022/043/NUSMed/25/LOA) to Y.I.

686

687 **CONFLICTS OF INTEREST**

688 The authors declare that they have no competing interest.

689 **REFERENCES**

690 Adachi M, Kawasaki A, Nojima H, Nishida E, Tsukita S (2014) Involvement of IQGAP family proteins in the
691 regulation of mammalian cell cytokinesis. Genes Cells 19: 803-20
692 Alberti S, Gladfelter A, Mittag T (2019) Considerations and Challenges in Studying Liquid-Liquid Phase
693 Separation and Biomolecular Condensates. Cell 176: 419-434
694 Banani SF, Rice AM, Peeples WB, Lin Y, Jain S, Parker R, Rosen MK (2016) Compositional Control of
695 Phase-Separated Cellular Bodies. Cell 166: 651-663
696 Barabasi AL, Gulbahce N, Loscalzo J (2011) Network medicine: a network-based approach to human
697 disease. Nat Rev Genet 12: 56-68
698 Bernkopf DB, Bruckner M, Hadjihannas MV, Behrens J (2019) An aggregon in conductin/axin2 regulates
699 Wnt/beta-catenin signaling and holds potential for cancer therapy. Nat Commun 10: 4251
700 Brandt DT, Grosse R (2007) Get to grips: steering local actin dynamics with IQGAPs. EMBO Rep 8: 1019-
701 23
702 Branon TC, Bosch JA, Sanchez AD, Udeshi ND, Svinkina T, Carr SA, Feldman JL, Perrimon N, Ting AY (2018)
703 Efficient proximity labeling in living cells and organisms with TurboID. Nat Biotechnol 36: 880-887
704 Caca K, Kolligs FT, Ji X, Hayes M, Qian J, Yahanda A, Rimm DL, Costa J, Fearon ER (1999) Beta- and
705 gamma-catenin mutations, but not E-cadherin inactivation, underlie T-cell factor/lymphoid enhancer
706 factor transcriptional deregulation in gastric and pancreatic cancer. Cell Growth Differ 10: 369-76
707 Caldeira J, Figueiredo J, Bras-Pereira C, Carneiro P, Moreira AM, Pinto MT, Relvas JB, Carneiro F, Barbosa
708 M, Casares F, Janody F, Seruca R (2015) E-cadherin-defective gastric cancer cells depend on Laminin to
709 survive and invade. Hum Mol Genet 24: 5891-900
710 Caldwell GM, Jones CE, Taniere P, Warrack R, Soon Y, Matthews GM, Morton DG (2006) The Wnt
711 antagonist sFRP1 is downregulated in premalignant large bowel adenomas. Br J Cancer 94: 922-7
712 Carmon KS, Gong X, Yi J, Thomas A, Liu Q (2014) RSPO-LGR4 functions via IQGAP1 to potentiate Wnt
713 signaling. Proc Natl Acad Sci U S A 111: E1221-9
714 Decker CJ, Parker R (2012) P-bodies and stress granules: possible roles in the control of translation and
715 mRNA degradation. Cold Spring Harb Perspect Biol 4: a012286
716 Denis CL, Chen J (2003) The CCR4-NOT complex plays diverse roles in mRNA metabolism. Prog Nucleic
717 Acid Res Mol Biol 73: 221-50
718 Dzijak R, Yildirim S, Kahle M, Novak P, Hnilicova J, Venit T, Hozak P (2012) Specific nuclear localizing
719 sequence directs two myosin isoforms to the cell nucleus in calmodulin-sensitive manner. PLoS One 7:
720 e30529
721 Esposito M, Fang C, Cook KC, Park N, Wei Y, Spadazzi C, Bracha D, Gunaratna RT, Laevsky G, DeCoste CJ,
722 Slabodkin H, Brangwynne CP, Cristea IM, Kang Y (2021) TGF-beta-induced DACT1 biomolecular
723 condensates repress Wnt signalling to promote bone metastasis. Nat Cell Biol 23: 257-267
724 Fiedler M, Mendoza-Topaz C, Rutherford TJ, Mieszczanek J, Bienz M (2011) Dishevelled interacts with
725 the DIX domain polymerization interface of Axin to interfere with its function in down-regulating beta-
726 catenin. Proc Natl Acad Sci U S A 108: 1937-42
727 Fischer C, Kugler A, Hoth S, Dietrich P (2013) An IQ domain mediates the interaction with calmodulin in a
728 plant cyclic nucleotide-gated channel. Plant Cell Physiol 54: 573-84
729 Ford LK, Fioriti L (2020) Coiled-Coil Motifs of RNA-Binding Proteins: Dynamicity in RNA Regulation. Front
730 Cell Dev Biol 8: 607947
731 Fox AD, Hescott BJ, Blumer AC, Slonim DK (2011) Connectedness of PPI network neighborhoods
732 identifies regulatory hub proteins. Bioinformatics 27: 1135-42
733 Goentoro L, Kirschner MW (2009) Evidence that fold-change, and not absolute level, of beta-catenin
734 dictates Wnt signaling. Mol Cell 36: 872-84
735 Goh JY, Feng M, Wang W, Oguz G, Yatim S, Lee PL, Bao Y, Lim TH, Wang P, Tam WL, Kodahl AR, Lyng MB,
736 Sarma S, Lin SY, Lezhava A, Yap YS, Lim AST, Hoon DSB, Ditzel HJ, Lee SC et al. (2017) Chromosome
737 1q21.3 amplification is a trackable biomarker and actionable target for breast cancer recurrence. Nat
738 Med 23: 1319-1330

739 He B, Reguart N, You L, Mazieres J, Xu Z, Lee AY, Mikami I, McCormick F, Jablons DM (2005) Blockade of
740 Wnt-1 signaling induces apoptosis in human colorectal cancer cells containing downstream mutations.
741 Oncogene 24: 3054-8
742 Hori A, Toda T (2017) Regulation of centriolar satellite integrity and its physiology. Cell Mol Life Sci 74:
743 213-229
744 Hu X, Wu X, Berry K, Zhao C, Xin D, Ogurek S, Liu X, Zhang L, Luo Z, Sakabe M, Trubicka J, Lastowska M,
745 Szulzewsky F, Holland EC, Lee L, Hu M, Xin M, Lu QR (2023) Nuclear condensates of YAP fusion proteins
746 alter transcription to drive ependymoma tumourigenesis. Nat Cell Biol 25: 323-336
747 Hyman AA, Weber CA, Julicher F (2014) Liquid-liquid phase separation in biology. Annu Rev Cell Dev Biol
748 30: 39-58
749 Jung YS, Park JI (2020) Wnt signaling in cancer: therapeutic targeting of Wnt signaling beyond beta-
750 catenin and the destruction complex. Exp Mol Med 52: 183-191
751 Kang K, Shi Q, Wang X, Chen YG (2022) Dishevelled phase separation promotes Wnt signalosome
752 assembly and destruction complex disassembly. J Cell Biol 221
753 Kuhnert F, Davis CR, Wang HT, Chu P, Lee M, Yuan J, Nusse R, Kuo CJ (2004) Essential requirement for
754 Wnt signaling in proliferation of adult small intestine and colon revealed by adenoviral expression of
755 Dickkopf-1. Proc Natl Acad Sci U S A 101: 266-71
756 Lach RS, Qiu C, Kajbaf EZ, Baxter N, Han D, Wang A, Lock H, Chirikian O, Pruitt B, Wilson MZ (2022)
757 Nucleation of the destruction complex on the centrosome accelerates degradation of beta-catenin and
758 regulates Wnt signal transmission. Proc Natl Acad Sci U S A 119: e2204688119
759 Lawo S, Bashkurov M, Mullin M, Ferreria MG, Kittler R, Habermann B, Tagliaferro A, Poser I, Hutchins JR,
760 Hegemann B, Pinchev D, Buchholz F, Peters JM, Hyman AA, Gingras AC, Pelletier L (2009) HAUS, the 8-
761 subunit human Augmin complex, regulates centrosome and spindle integrity. Curr Biol 19: 816-26
762 Leung JY, Kolligs FT, Wu R, Zhai Y, Kuick R, Hanash S, Cho KR, Fearon ER (2002) Activation of AXIN2
763 expression by beta-catenin-T cell factor. A feedback repressor pathway regulating Wnt signaling. J Biol
764 Chem 277: 21657-65
765 Leushacke M, Tan SH, Wong A, Swathi Y, Hajamohideen A, Tan LT, Goh J, Wong E, Denil S, Murakami K,
766 Barker N (2017) Lgr5-expressing chief cells drive epithelial regeneration and cancer in the oxyntic
767 stomach. Nat Cell Biol 19: 774-786
768 Li VS, Ng SS, Boersema PJ, Low TY, Karthaus WR, Gerlach JP, Mohammed S, Heck AJ, Maurice MM,
769 Mahmoudi T, Clevers H (2012) Wnt signaling through inhibition of beta-catenin degradation in an intact
770 Axin1 complex. Cell 149: 1245-56
771 Liang M, Jin G, Xie X, Zhang W, Li K, Niu F, Yu C, Wei Z (2021) Oligomerized liprin-alpha promotes phase
772 separation of ELKS for compartmentalization of presynaptic active zone proteins. Cell Rep 34: 108901
773 Lin M, Liu Y, Ding X, Ke Q, Shi J, Ma Z, Gu H, Wang H, Zhang C, Yang C, Fang Z, Zhou L, Ye M (2019) E2F1
774 transactivates IQGAP3 and promotes proliferation of hepatocellular carcinoma cells through IQGAP3-
775 mediated PKC-alpha activation. Am J Cancer Res 9: 285-299
776 Lu Y, Wu T, Gutman O, Lu H, Zhou Q, Henis YI, Luo K (2020) Phase separation of TAZ compartmentalizes
777 the transcription machinery to promote gene expression. Nat Cell Biol 22: 453-464
778 Mao S, Liu Q, Wu H, Zhu J, Xie Y, Ma J, Zhen N, Pan Q (2023) Phase separation of YAP mediated by
779 coiled-coil domain promotes hepatoblastoma proliferation via activation of transcription. J
780 Gastroenterol Hepatol
781 Marin O, Bustos VH, Cesaro L, Meggio F, Pagano MA, Antonelli M, Allende CC, Pinna LA, Allende JE (2003)
782 A noncanonical sequence phosphorylated by casein kinase 1 in beta-catenin may play a role in casein
783 kinase 1 targeting of important signaling proteins. Proc Natl Acad Sci U S A 100: 10193-200
784 Matsuo J, Douchi D, Myint K, Mon NN, Yamamura A, Kohu K, Heng DL, Chen S, Mawan NA, Nuttonmanit
785 N, Li Y, Srivastava S, Ho SWT, Lee NYS, Lee HK, Adachi M, Tamura A, Chen J, Yang H, Teh M et al. (2020)
786 Iqgap3-Ras axis drives stem cell proliferation in the stomach corpus during homoeostasis and repair. Gut
787 Matsuo J, Douchi D, Myint K, Mon NN, Yamamura A, Kohu K, Heng DL, Chen S, Mawan NA, Nuttonmanit
788 N, Li Y, Srivastava S, Ho SWT, Lee NYS, Lee HK, Adachi M, Tamura A, Chen J, Yang H, Teh M et al. (2021)

789 Iqgap3-Ras axis drives stem cell proliferation in the stomach corpus during homoeostasis and repair. Gut
790 70: 1833-1846
791 Mehta S, Zhang J (2022) Liquid-liquid phase separation drives cellular function and dysfunction in cancer.
792 Nat Rev Cancer 22: 239-252
793 Meng F, Yu Z, Zhang D, Chen S, Guan H, Zhou R, Wu Q, Zhang Q, Liu S, Venkat Ramani MK, Yang B, Ba XQ,
794 Zhang J, Huang J, Bai X, Qin J, Feng XH, Ouyang S, Zhang YJ, Liang T et al. (2021) Induced phase
795 separation of mutant NF2 imprisons the cGAS-STING machinery to abrogate antitumor immunity. Mol
796 Cell 81: 4147-4164 e7
797 Monteleon CL, McNeal A, Duperret EK, Oh SJ, Schapira E, Ridky TW (2015) IQGAP1 and IQGAP3 Serve
798 Individually Essential Roles in Normal Epidermal Homeostasis and Tumor Progression. J Invest Dermatol
799 135: 2258-2265
800 Muzzopappa F, Hummert J, Anfossi M, Tashev SA, Herten DP, Erdel F (2022) Detecting and quantifying
801 liquid-liquid phase separation in living cells by model-free calibrated half-bleaching. Nat Commun 13:
802 7787
803 Myint K, Chuang LSH, Teh YX, Mawan NA, Shi EJ, Mok MMH, Nuttonmanit N, Matsuo J, Li Y, Yang H,
804 Okabe A, Kaneda A, Osato M, So JB, Yong WP, Tan P, Yeoh KG, Ito Y (2022) Oncofetal protein IGF2BP1
805 regulates IQGAP3 expression to maintain stem cell potential in cancer. iScience 25: 105194
806 Nesterov SV, Ilyinsky NS, Uversky VN (2021) Liquid-liquid phase separation as a common organizing
807 principle of intracellular space and biomembranes providing dynamic adaptive responses. Biochim
808 Biophys Acta Mol Cell Res 1868: 119102
809 Newton JC, Naik MT, Li GY, Murphy EL, Fawzi NL, Sedivy JM, Jogl G (2021) Phase separation of the LINE-1
810 ORF1 protein is mediated by the N-terminus and coiled-coil domain. Biophys J 120: 2181-2191
811 Niehrs C, Acebron SP (2012) Mitotic and mitogenic Wnt signalling. EMBO J 31: 2705-13
812 Niida A, Hiroko T, Kasai M, Furukawa Y, Nakamura Y, Suzuki Y, Sugano S, Akiyama T (2004) DKK1, a
813 negative regulator of Wnt signaling, is a target of the beta-catenin/TCF pathway. Oncogene 23: 8520-6
814 Nojima H, Adachi M, Matsui T, Okawa K, Tsukita S, Tsukita S (2008) IQGAP3 regulates cell proliferation
815 through the Ras/ERK signalling cascade. Nat Cell Biol 10: 971-8
816 Nong J, Kang K, Shi Q, Zhu X, Tao Q, Chen YG (2021) Phase separation of Axin organizes the beta-catenin
817 destruction complex. J Cell Biol 220
818 Nusse R (2008) Wnt signaling and stem cell control. Cell Res 18: 523-7
819 Polakis P (2012) Wnt signaling in cancer. Cold Spring Harb Perspect Biol 4
820 Poudyal M, Patel K, Gadhe L, Sawner AS, Kadu P, Datta D, Mukherjee S, Ray S, Navalkar A, Maiti S,
821 Chatterjee D, Devi J, Bera R, Gahlot N, Joseph J, Padinhateeri R, Maji SK (2023) Intermolecular
822 interactions underlie protein/peptide phase separation irrespective of sequence and structure at
823 crowded milieu. Nat Commun 14: 6199
824 Ramakrishnan AB, Cadigan KM (2017) Wnt target genes and where to find them. F1000Res 6: 746
825 Ring A, Kim YM, Kahn M (2014) Wnt/catenin signaling in adult stem cell physiology and disease. Stem
826 Cell Rev Rep 10: 512-25
827 Sanchez-Laorden B, Viros A, Marais R (2013) Mind the IQGAP. Cancer Cell 23: 715-7
828 Sanjana NE, Shalem O, Zhang F (2014) Improved vectors and genome-wide libraries for CRISPR screening.
829 Nat Methods 11: 783-784
830 Schaefer KN, Peifer M (2019) Wnt/Beta-Catenin Signaling Regulation and a Role for Biomolecular
831 Condensates. Dev Cell 48: 429-444
832 Schmitt M, Metzger M, Gradl D, Davidson G, Orian-Rousseau V (2015) CD44 functions in Wnt signaling
833 by regulating LRP6 localization and activation. Cell Death Differ 22: 677-89
834 Shakya A, Park S, Rana N, King JT (2020) Liquid-Liquid Phase Separation of Histone Proteins in Cells: Role
835 in Chromatin Organization. Biophys J 118: 753-764
836 Shi Q, Kang K, Chen YG (2021) Liquid-liquid phase separation drives the beta-catenin destruction
837 complex formation. Bioessays 43: e2100138

838 Stelzl U, Worm U, Lalowski M, Haenig C, Brembeck FH, Goehler H, Stroedicke M, Zenkner M, Schoenherr
839 A, Koeppen S, Timm J, Mintzlaff S, Abraham C, Bock N, Kietzmann S, Goedde A, Toksoz E, Droege A,
840 Krobitsch S, Korn B et al. (2005) A human protein-protein interaction network: a resource for annotating
841 the proteome. Cell 122: 957-68
842 Tong X, Tang R, Xu J, Wang W, Zhao Y, Yu X, Shi S (2022) Liquid-liquid phase separation in tumor biology.
843 Signal Transduct Target Ther 7: 221
844 Tuupanen S, Turunen M, Lehtonen R, Hallikas O, Vanharanta S, Kivioja T, Bjorklund M, Wei G, Yan J,
845 Niittymaki I, Mecklin JP, Jarvinen H, Ristimaki A, Di-Bernardo M, East P, Carvajal-Carmona L, Houlston RS,
846 Tomlinson I, Palin K, Ukkonen E et al. (2009) The common colorectal cancer predisposition SNP
847 rs6983267 at chromosome 8q24 confers potential to enhanced Wnt signaling. Nat Genet 41: 885-90
848 Valenta T, Hausmann G, Basler K (2012) The many faces and functions of beta-catenin. EMBO J 31: 2714-
849 36
850 van de Wetering M, Clevers H (1992) Sequence-specific interaction of the HMG box proteins TCF-1 and
851 SRY occurs within the minor groove of a Watson-Crick double helix. EMBO J 11: 3039-44
852 van de Wetering M, Sancho E, Verweij C, de Lau W, Oving I, Hurlstone A, van der Horn K, Batlle E,
853 Coudreuse D, Haramis AP, Tjon-Pon-Fong M, Moerer P, van den Born M, Soete G, Pals S, Eilers M,
854 Medema R, Clevers H (2002) The beta-catenin/TCF-4 complex imposes a crypt progenitor phenotype on
855 colorectal cancer cells. Cell 111: 241-50
856 van Es JH, Haegebarth A, Kujala P, Itzkovitz S, Koo BK, Boj SF, Korving J, van den Born M, van
857 Oudenaarden A, Robine S, Clevers H (2012) A critical role for the Wnt effector Tcf4 in adult intestinal
858 homeostatic self-renewal. Mol Cell Biol 32: 1918-27
859 Van Raay TJ, Coffey RJ, Solnica-Krezel L (2007) Zebrafish Naked1 and Naked2 antagonize both canonical
860 and non-canonical Wnt signaling. Dev Biol 309: 151-68
861 Vazquez-Mena O, Medina-Martinez I, Juarez-Torres E, Barron V, Espinosa A, Villegas-Sepulveda N,
862 Gomez-Laguna L, Nieto-Martinez K, Orozco L, Roman-Basaure E, Munoz Cortez S, Borges Ibanez M,
863 Venegas-Vega C, Guardado-Estrada M, Rangel-Lopez A, Kofman S, Berumen J (2012) Amplified genes
864 may be overexpressed, unchanged, or downregulated in cervical cancer cell lines. PLoS One 7: e32667
865 Wang L, Choi K, Su T, Li B, Wu X, Zhang R, Driskill JH, Li H, Lei H, Guo P, Chen EH, Zheng Y, Pan D (2022)
866 Multiphase coalescence mediates Hippo pathway activation. Cell 185: 4376-4393 e18
867 Wang S, Watanabe T, Noritake J, Fukata M, Yoshimura T, Itoh N, Harada T, Nakagawa M, Matsuura Y,
868 Arimura N, Kaibuchi K (2007) IQGAP3, a novel effector of Rac1 and Cdc42, regulates neurite outgrowth. J
869 Cell Sci 120: 567-77
870 Wells CD, Fawcett JP, Traweger A, Yamanaka Y, Goudreault M, Elder K, Kulkarni S, Gish G, Virag C, Lim C,
871 Colwill K, Starostine A, Metalnikov P, Pawson T (2006) A Rich1/Amot complex regulates the Cdc42
872 GTPase and apical-polarity proteins in epithelial cells. Cell 125: 535-48
873 Xu W, Xu B, Yao Y, Yu X, Cao H, Zhang J, Liu J, Sheng H (2016) Overexpression and biological function of
874 IQGAP3 in human pancreatic cancer. Am J Transl Res 8: 5421-5432
875 Yang Y, Zhao W, Xu QW, Wang XS, Zhang Y, Zhang J (2014) IQGAP3 promotes EGFR-ERK signaling and the
876 growth and metastasis of lung cancer cells. PLoS One 9: e97578
877 Zamudio AV, Dall'Agnese A, Henninger JE, Manteiga JC, Afeyan LK, Hannett NM, Coffey EL, Li CH, Oksuz
878 O, Sabari BR, Boija A, Klein IA, Hawken SW, Spille JH, Decker TM, Cisse, II, Abraham BJ, Lee TI, Taatjes DJ,
879 Schuijers J et al. (2019) Mediator Condensates Localize Signaling Factors to Key Cell Identity Genes. Mol
880 Cell 76: 753-766 e6
881 Zhong Z, Virshup DM (2020) Wnt Signaling and Drug Resistance in Cancer. Mol Pharmacol 97: 72-89

882

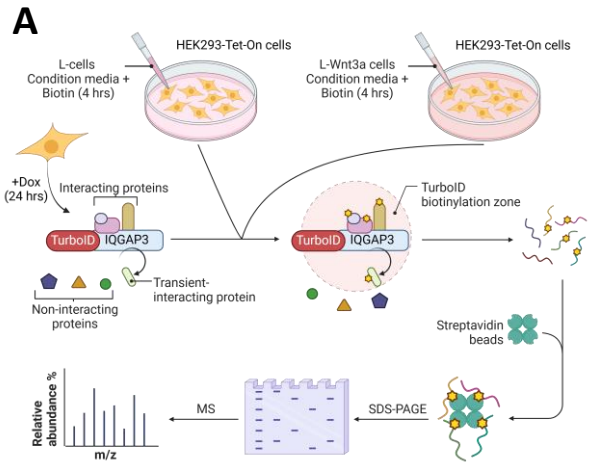
A
HEK293-Tet-On cells
L-cells
Condition media +
Biotin (4 hrs)
HEK293-Tet-On cells
L-Wnt3a cells
Condition media +
Biotin (4 hrs)
+Dox
(24 hrs)
Interacting proteins
TurboID
IQGAP3
TurboID
IQGAP3
TurboID
biotinylation zone
Transient-
interacting protein
Non-interacting
proteins
Streptavidin
beads
Relative
abundance %
m/z
MS
SDS-PAGE

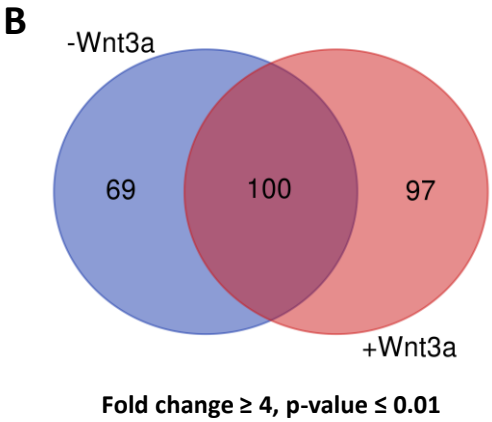
B
-Wnt3a
69
100
97
+Wnt3a
Fold change ≥ 4, p-value ≤ 0.01

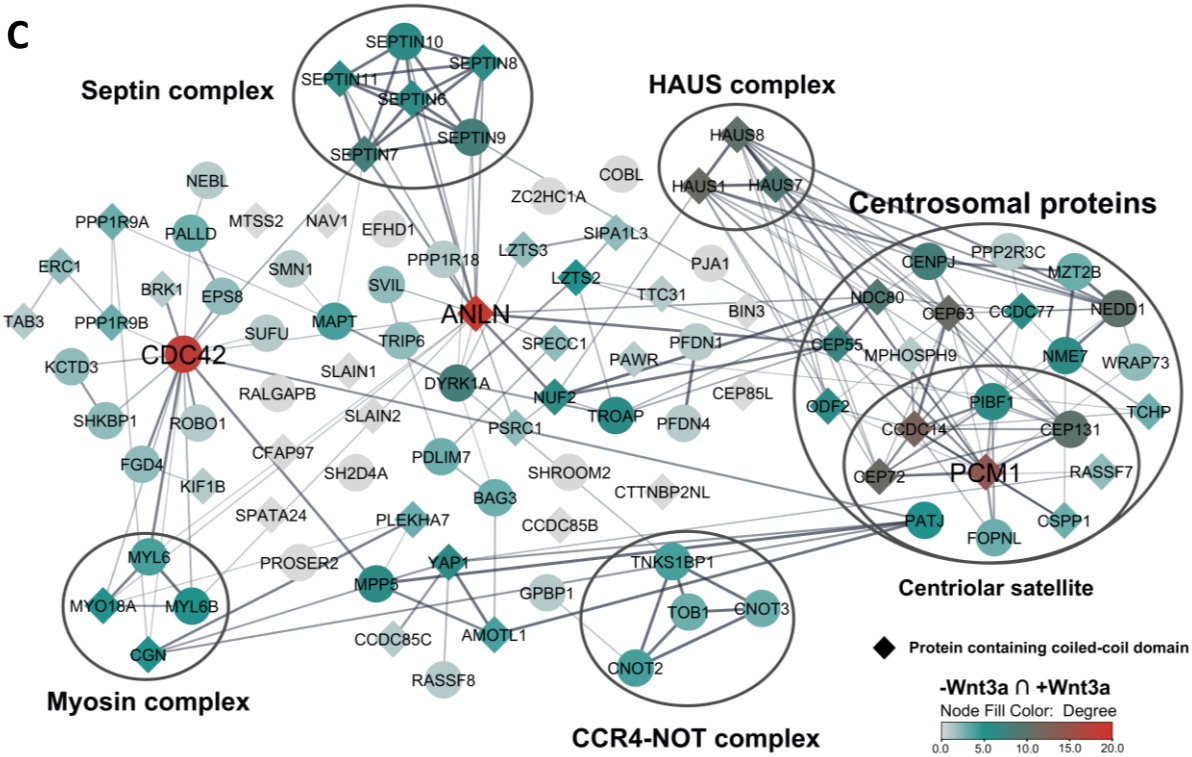
C
Septin complex
SEPTIN10
SEPTIN8
SEPTIN11
SEPTIN6
SEPTIN9
SEPTIN7
HAUS complex
HAUS8
HAUS1
HAUS7
Centrosomal proteins
NEBL
COBL
ZC2HC1A
PPP1R9A
PALLD
MTSS2
NAV1
EFHD1
SIPA1L3
LZTS3
PPP1R18
PJA1
ERC1
SMN1
LZTS2
BRK1
EPS8
SVIL
TTC31
TAB3
PPP1R9B
SUFU
MAPT
ANLN
BIN3
CDC42
TRIP6
SPECC1
PFDN1
KCTD3
SLAIN1
PAWR
DYRK1A
RALGAPB
NUF2
CEP85L
SHKBP1
ROBO1
SLAIN2
TROAP
PFDN4
PSRC1
FGD4
CFAP97
PDLIM7
KIF1B
SH2D4A
SHROOM2
CTTNBP2NL
BAG3
SPATA24
PLEKHA7
CCDC85B
PROSER2
YAP1
MPP5
GPBP1
AMOTL1
CCDC85C
RASSF8
MYL6
MYO18A
MYL6B
CGN
Myosin complex
TNKS1BP1
TOB1
CNOT3
CNOT2
CCR4-NOT complex
CENPJ
PPP2R3C
MZT2B
NDC80
CEP63
CCDC77
NEDD1
CEP55
MPHOSPHH9
NME7
WRAP73
ODF2
PIBF1
TCHP
CCDC14
CEP131
CEP72
PCM1
RASSF7
PATJ
CSPP1
FOPNL
Centriolar satellite
Protein containing coiled-coil domain
-Wnt3a ∩ +Wnt3a
Node Fill Color: Degree
0.0
5.0
10.0
15.0
20.0

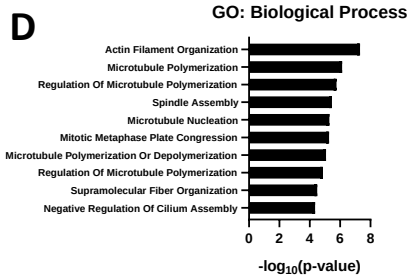
D
GO: Biological Process
Actin Filament Organization
Microtubule Polymerization
Regulation Of Microtubule Polymerization
Spindle Assembly
Microtubule Nucleation
Mitotic Metaphase Plate Congression
Microtubule Polymerization Or Depolymerization
Regulation Of Microtubule Polymerization
Supramolecular Fiber Organization
Negative Regulation Of Cilium Assembly
0
2
4
6
8
-log10(p-value)

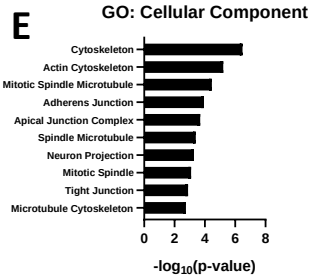
E
GO: Cellular Component
Cytoskeleton
Actin Cytoskeleton
Mitotic Spindle Microtubule
Adherens Junction
Apical Junction Complex
Spindle Microtubule
Neuron Projection
Mitotic Spindle
Tight Junction
Microtubule Cytoskeleton
0
2
4
6
8
-log10(p-value)

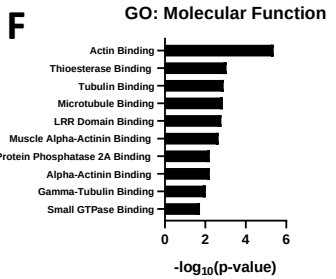
F
GO: Molecular Function
Actin Binding
Thioesterase Binding
Tubulin Binding
Microtubule Binding
LRR Domain Binding
Muscle Alpha-Actinin Binding
Protein Phosphatase 2A Binding
Alpha-Actinin Binding
Gamma-Tubulin Binding
Small GTPase Binding
0
2
4
6
-log10(p-value)

Fig. 1. Proximity proteomics reveal IQGAP3 interaction with Cdc42, Anillin and with centrosome- and septin-complexes. (A) Workflow for proximity-dependent identification of IQGAP3-associated proteins in HEK293 cells treated with either L-cells condition media (-Wnt3a) or L-Wnt3a cells condition media (+Wnt3a) treatment for 4 hours, Created with BioRender.com. (B) Venn diagram of biotinylated proteins detected in HEK293 cells treated with L-cells condition media (-Wnt3a) and L-Wnt3a cells condition media (+Wnt3a) (Fold change ≥ 4, p-value ≤ 0.01). (C) Interactome of -Wnt3a ∩ +Wnt3a (Fold change ≥ 4, p-value ≤ 0.01), node color denote degree distribution, Created with Cytoscape. (D) Gene ontology: Biological Process of shared proximity partners in -Wnt3a and +Wnt3a treated cells. (E) Gene ontology: Molecular function of shared proximity partners in -Wnt3a and +Wnt3a treated cells. (F) Gene ontology: Cellular compartment of shared proximity partners in -Wnt3a and +Wnt3a treated cells.

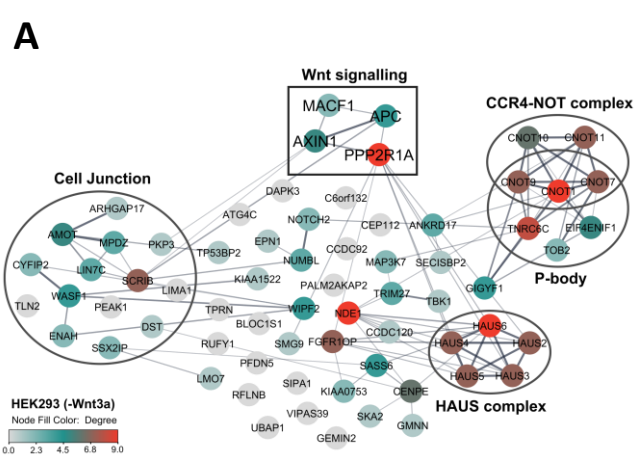
A
Wnt signalling
MACF1
APC
AXIN1
PPP2R1A
CCR4-NOT complex
CNOT10
CNOT11
CNOT9
CNOT1
CNOT7
TNRC6C
EIF4ENIF1
TOB2
P-body
Cell Junction
ARHGAP17
AMOT
MPDZ
PKP3
CYFIP2
LIN7C
SCRIB
WASF1
LIMA1
TLN2
PEAK1
ENAH
DST
SSX2IP
DAPK3
ATG4C
C6orf132
NOTCH2
EPN1
TP53BP2
CEP112
ANKRD17
CCDC92
NUMBL
MAP3K7
SECISBP2
KIAA1522
PALM2AKAP2
TRIM27
TBK1
GIGYF1
TPRN
WIPF2
NDE1
BLOC1S1
CCDC120
RUFY1
SMG9
FGFR10P
HAUS6
HAUS4
HAUS2
HAUS5
HAUS3
PFDN5
SASS6
LMO7
SIPA1
KIAA0753
CENPE
RFLNB
VIPAS39
SKA2
GMNN
UBAP1
GEMIN2
HAUS complex
HEK293 (-Wnt3a)
Node Fill Color: Degree
0.0 2.3 4.5 6.8 9.0

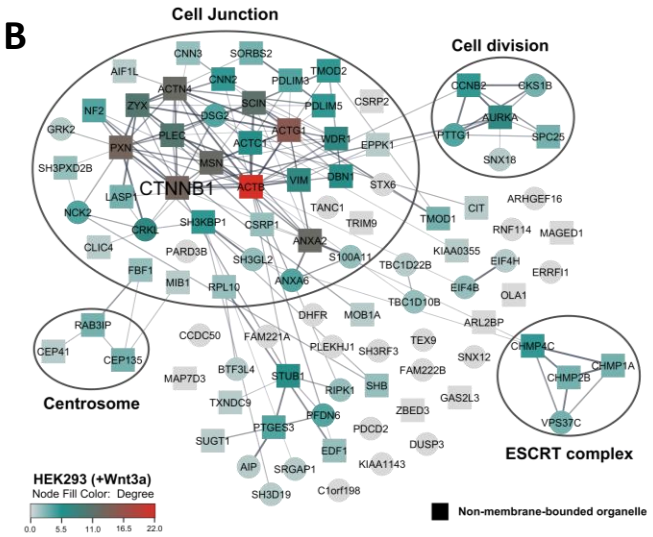
B
Cell Junction
CTNNB1
Cell division
CCNB2
CKS1B
AURKA
FTTG1
SPC25
SNX18
Centrosome
RAB3IP
CEP41
CEP135
ESCRT complex
CHMP4C
CHMP1A
CHMP2B
VPS37C
HEK293 (+Wnt3a)
Node Fill Color: Degree
0.0 5.5 11.0 16.5 22.0
Non-membrane-bounded organelle

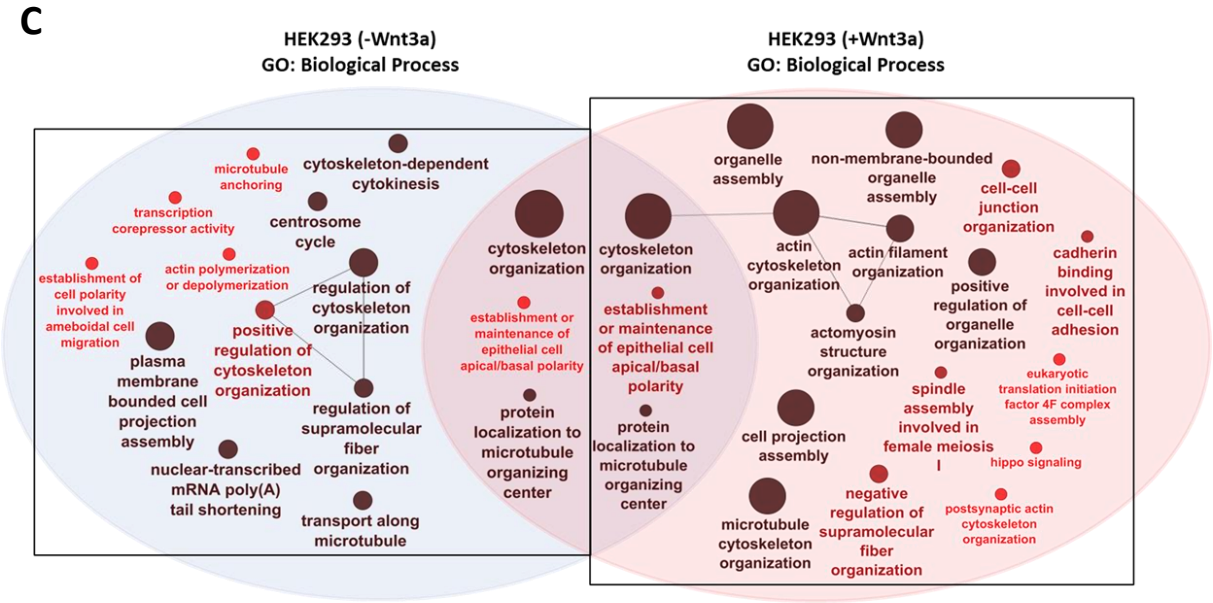
C
HEK293 (-Wnt3a)
GO: Biological Process
microtubule anchoring
cytoskeleton-dependent cytokinesis
transcription corepressor activity
centrosome cycle
establishment of cell polarity involved in ameboidal cell migration
actin polymerization or depolymerization
regulation of cytoskeleton organization
positive regulation of cytoskeleton organization
plasma membrane bounded cell projection assembly
regulation of supramolecular fiber organization
nuclear-transcribed mRNA poly(A) tail shortening
transport along microtubule
HEK293 (+Wnt3a)
GO: Biological Process
cytoskeleton organization
establishment or maintenance of epithelial cell apical/basal polarity
protein localization to microtubule organizing center
organelle assembly
non-membrane-bounded organelle assembly
cell-cell junction organization
actin cytoskeleton organization
actin filament organization
cadherin binding involved in cell-cell adhesion
positive regulation of organelle organization
actomyosin structure organization
spindle assembly involved in female meiosis I
eukaryotic translation initiation factor 4F complex assembly
cell projection assembly
hippo signaling
negative regulation of supramolecular fiber organization
postsynaptic actin cytoskeleton organization
microtubule cytoskeleton organization

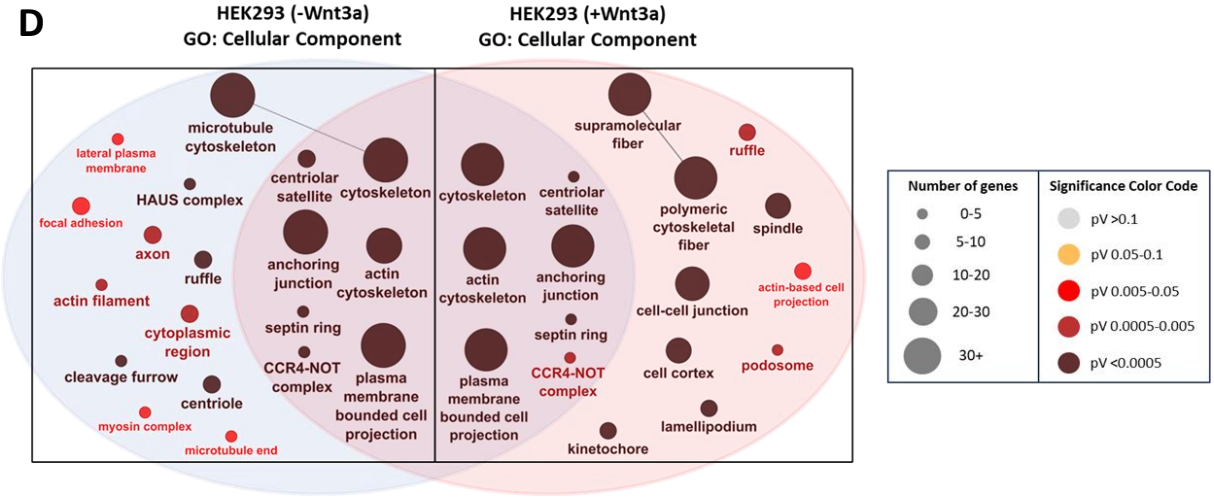
D
HEK293 (-Wnt3a)
GO: Cellular Component
HEK293 (+Wnt3a)
GO: Cellular Component
microtubule cytoskeleton
lateral plasma membrane
HAUS complex
focal adhesion
axon
ruffle
actin filament
cytoplasmic region
cleavage furrow
centriole
myosin complex
microtubule end
centriolar satellite
cytoskeleton
anchoring junction
actin cytoskeleton
septin ring
CCR4-NOT complex
plasma membrane bounded cell projection
supramolecular fiber
ruffle
polymeric cytoskeletal fiber
spindle
actin-based cell projection
cell-cell junction
cell cortex
podosome
lamellipodium
kinetochore
Number of genes
0-5
5-10
10-20
20-30
30+
Significance Color Code
pV >0.1
pV 0.05-0.1
pV 0.005-0.05
pV 0.0005-0.005
pV <0.0005

Fig. 2. Wnt3a treatment promotes IQGAP3 localization to non-membrane organelles and cell junctions. (A) IQGAP3-biotinylated proteins exclusively found in cells treated with L-cells conditioned media (-Wnt3a). Shown are proximity partners with Fold change ≥ 4, p-value ≤ 0.01, node color denote degree distribution, Created with Cytoscape. (B) IQGAP3-biotinylated proteins exclusively found in cells treated with L-Wnt3a cells conditioned media (+Wnt3a). Shown are proximity partners with Fold change ≥ 4, p-value ≤ 0.01, node color denote degree distribution, Created with Cytoscape. (C) ClueGO analysis for Biological Process enrichment of biotinylated protein in HEK293 cells treated with -Wnt3a and +Wnt3a conditioned media. Size denote number of mapped genes and node color denote p-values. (D) ClueGO analysis for Cellular Compartment enrichment of biotinylated protein in HEK293 cells treated with -Wnt3a and +Wnt3a conditioned media. Size denote number of mapped genes and node color denote p-values.

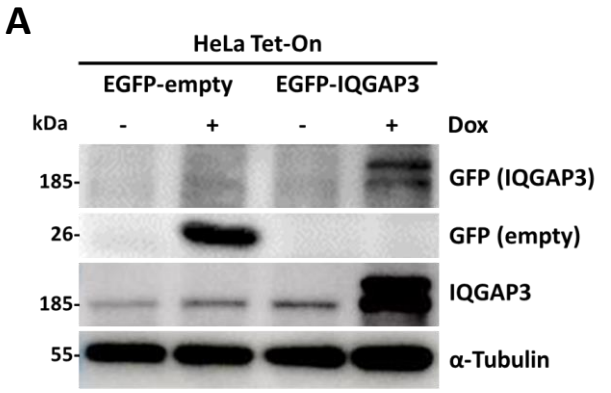
A
HeLa Tet-On
EGFP-empty
EGFP-IQGAP3
kDa
-
+
-
+
Dox
185-
GFP (IQGAP3)
26-
GFP (empty)
185-
IQGAP3
55-
α-Tubulin

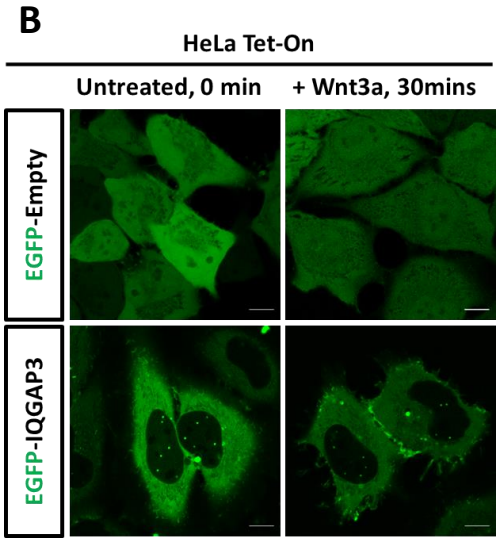
B
HeLa Tet-On
Untreated, 0 min
+ Wnt3a, 30mins
EGFP-Empty
EGFP-IQGAP3

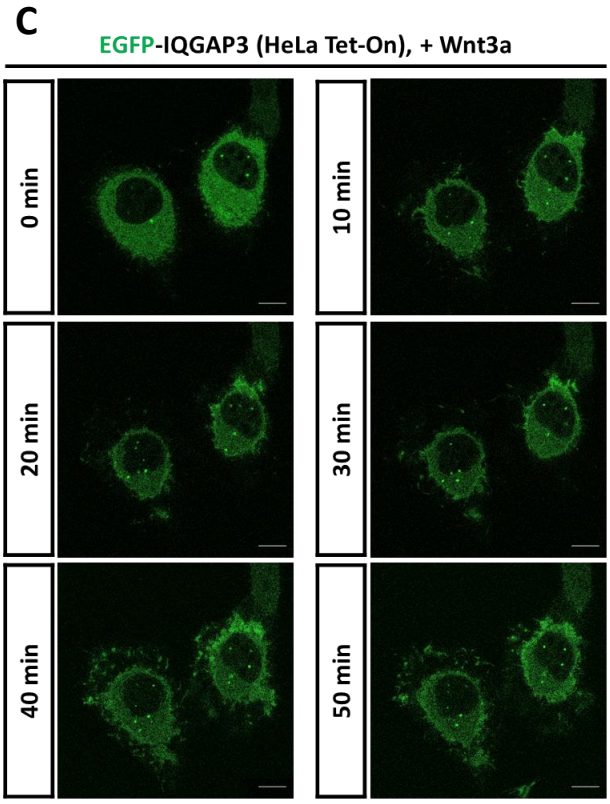
C
EGFP-IQGAP3 (HeLa Tet-On), + Wnt3a
0 min
10 min
20 min
30 min
40 min
50 min

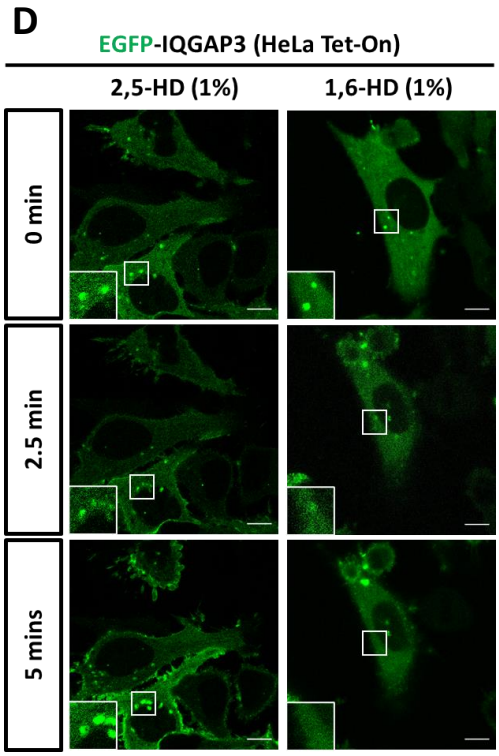
D
EGFP-IQGAP3 (HeLa Tet-On)
2,5-HD (1%)
1,6-HD (1%)
0 min
2.5 min
5 mins

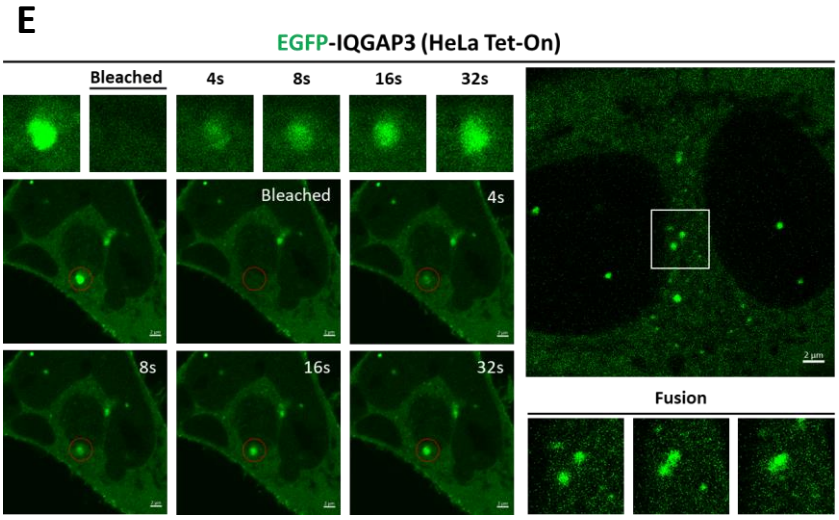
E
EGFP-IQGAP3 (HeLa Tet-On)
Bleached
4s
8s
16s
32s
Bleached
4s
8s
16s
32s
Fusion

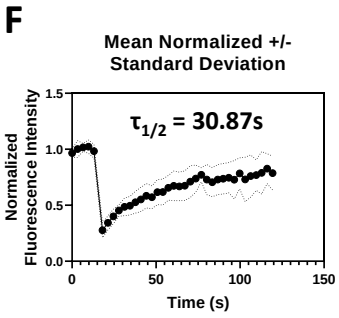
F
Mean Normalized +/-
Standard Deviation
$\tau_{1/2}$ = 30.87s
Normalized
Fluorescence Intensity
1.5
1.0
0.5
0.0
0
50
100
150
Time (s)

Fig. 3. IQGAP3 undergoes phase separation *in vivo*. (A) Immunoblot analysis of Doxycycline induction in HeLa Tet-On cells. Cells were induced with Doxycycline for 48 hours prior to cell lysis. (B) Live images of HeLa Tet-On cells expressing EGFP-empty and EGFP-IQGAP3 without and with Wnt3a treatment after 30 minutes. Cells were induced with Doxycycline for 48 hours prior to imaging. Images of untreated and post-treated cells are not the same cells but are the best representative examples. Scale bars, 10 µm. (C) Timelapse images of HeLa Tet-On cells expressing EGFP-IQGAP3 0 - 50 minutes post-Wnt3a treatment. Cells were induced with Doxycycline for 48 hours prior to imaging. Images of untreated and post-treated cells are the same cells (refer to timelapse video in supplementary). Scale bars, 10 µm. (D) Timelapse images of HeLa Tet-On cells expressing EGFP-IQGAP3 treated with either 1% 2,5-Hexanediol (control) or 1% 1,6-Hexanediol for 0-5 minutes. Images of untreated and post-treated cells are the same cells (refer to timelapse video in supplementary). Scale bars, 10 µm. (E) HeLa Tet-On cells stably expressing EGFP-IQGAP3 were subjected to FRAP bleaching and observed for recovery and fusion events. (For FRAP video refer to supplementary). Scale bars, 2 µm. (F) Mean normalized standard deviation of FRAP recovery of 5 bleached EGFP-IQGAP3 condensates, half time of recovery ($\tau 1/2$) = 30.87s.

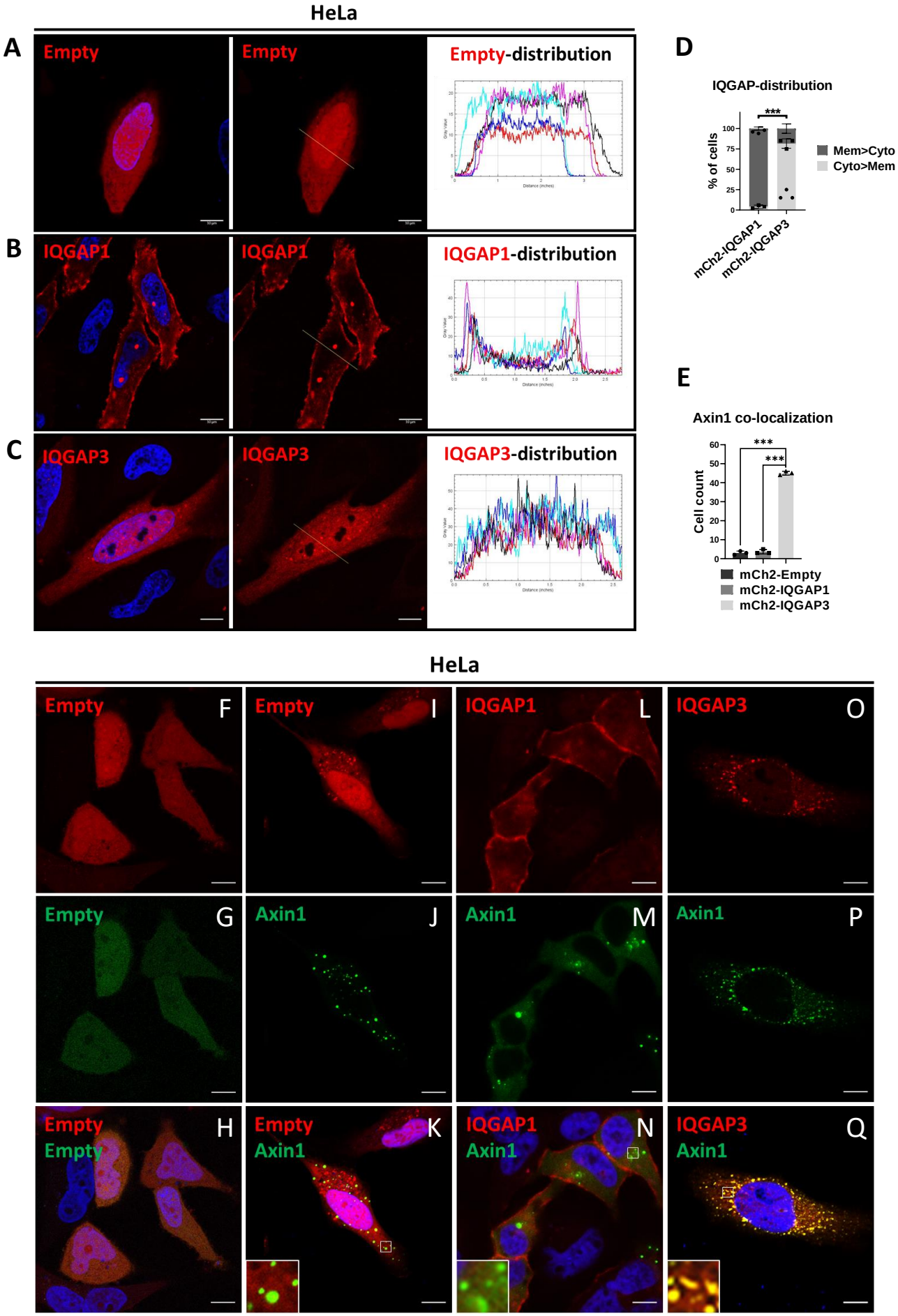
HeLa
A
Empty
Empty
Empty-distribution
B
IQGAP1
IQGAP1
IQGAP1-distribution
C
IQGAP3
IQGAP3
IQGAP3-distribution
D
IQGAP-distribution
***
% of cells
100
75
50
25
0
Mem>Cyto
Cyto>Mem
mCh2-IQGAP1
mCh2-IQGAP3
E
Axin1 co-localization
***
***
Cell count
60
50
40
30
20
10
0
mCh2-Empty
mCh2-IQGAP1
mCh2-IQGAP3
HeLa
Empty
F
Empty
I
IQGAP1
L
IQGAP3
O
Empty
G
Axin1
J
Axin1
M
Axin1
P
Empty
Empty
H
Empty
Axin1
K
IQGAP1
Axin1
N
IQGAP3
Axin1
Q

Fig. 4. IQGAP3 co-localizes with Axin1 puncta in the cytosol. HeLa cells were transfected with (A) mCherry2-empty and Cross-sectional line for Intensity plot measurement from 5 different cells (right). (B) mCherry-IQGAP1 and Cross-sectional line for Intensity plot measurement from 5 different cells (right). (C) mCherry2-IQGAP3 and Cross-sectional line for Intensity plot measurement from 5 different cells (right). Scale bars, 10 µm. (D) Percentile of cell count for IQGAP-distribution, cells with higher membrane intensity were counted as Membrane > Cytosol (Mem > Cyto) vice versa. Cell count for IQGAP distribution, 50 cells per sample. Representative data were collected and are expressed as the mean ± SD from three independent experiments (n=3). (E) Cell count for IQGAP-Axin1 co-localization, 50 cells per sample. Representative data were collected and are expressed as the mean ± SD from three independent experiments (n=3). Student's t test was performed, with $*p < 0.05$, $**p < 0.01$, and $***p < 0.001$. HeLa cells were transfected with (F-H) mCherry2-empty with EGFP-empty (negative control), (I-K) mCherry2-empty with EGFP-Axin1, (L-N) mCherry2-IQGAP1 with EGFP-Axin1, and (O-Q) mCherry2-IQGAP3 with EGFP-Axin1. Scale bars, 10 µm.

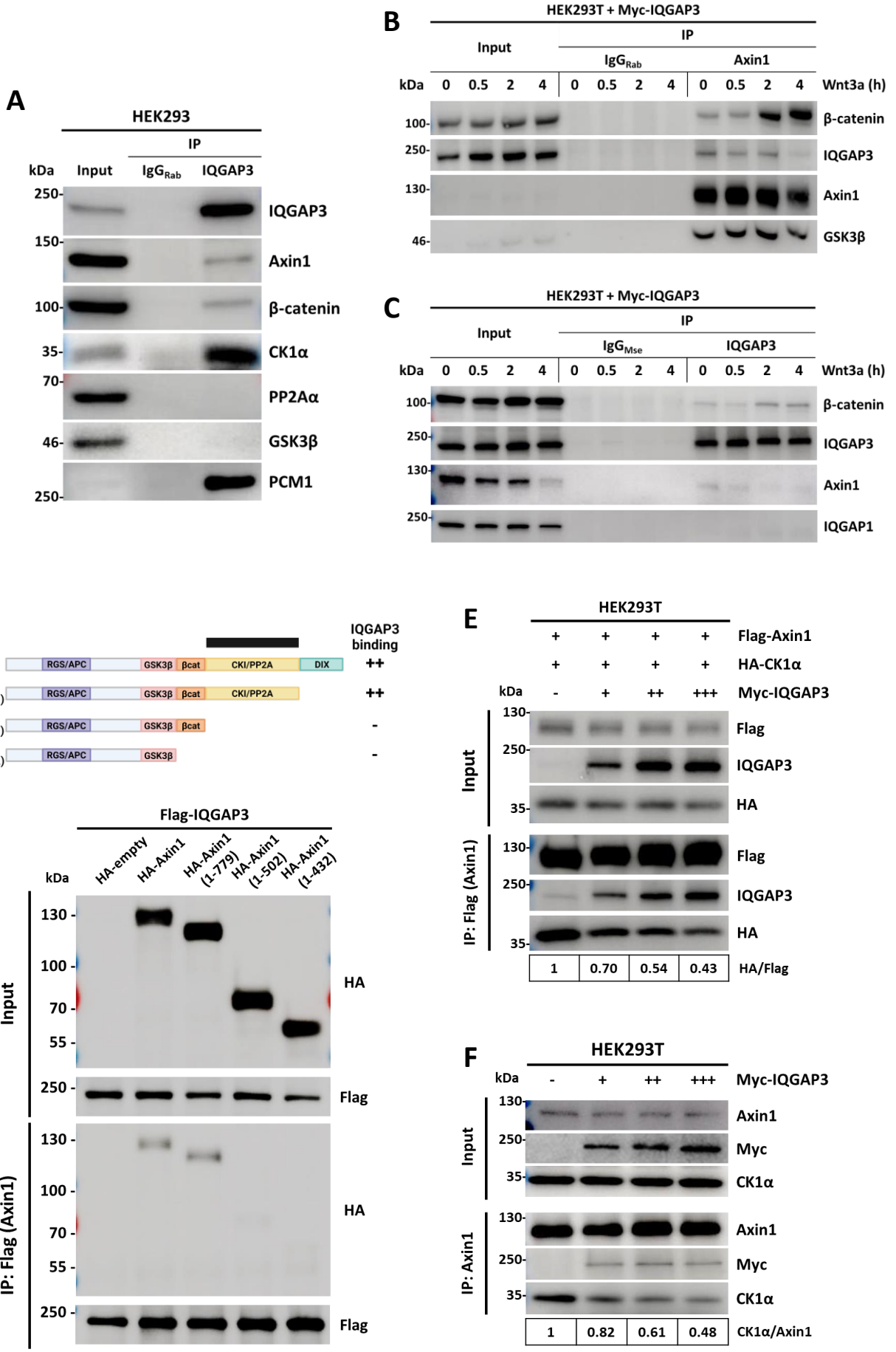
A
HEK293
IP
kDa
Input
IgG$_{Rab}$
IQGAP3
250-
150-
100-
35-
70-
46-
250-
IQGAP3
Axin1
β-catenin
CK1α
PP2Aα
GSK3β
PCM1
B
HEK293T + Myc-IQGAP3
Input
IP
IgG$_{Rab}$
Axin1
kDa
0 0.5 2 4 0 0.5 2 4 0 0.5 2 4
Wnt3a (h)
100-
250-
130-
46-
β-catenin
IQGAP3
Axin1
GSK3β
C
HEK293T + Myc-IQGAP3
Input
IP
IgG$_{Mse}$
IQGAP3
kDa
0 0.5 2 4 0 0.5 2 4 0 0.5 2 4
Wnt3a (h)
100-
250-
130-
250-
β-catenin
IQGAP3
Axin1
IQGAP1
D
IQGAP3 binding
Axin1 (FL)
RGS/APC
GSK3β
βcat
CKI/PP2A
DIX
++
Axin1 (1-779)
RGS/APC
GSK3β
βcat
CKI/PP2A
++
Axin1 (1-502)
RGS/APC
GSK3β
βcat
-
Axin1 (1-432)
RGS/APC
GSK3β
-
Flag-IQGAP3
HA-empty
HA-Axin1
HA-Axin1 (1-779)
HA-Axin1 (1-502)
HA-Axin1 (1-432)
kDa
Input
130 -
100 -
70 -
55 -
HA
250 -
Flag
IP: Flag (Axin1)
130 -
100 -
70 -
55 -
HA
250 -
Flag
E
HEK293T
Flag-Axin1
HA-CK1α
kDa
- + ++ +++
Myc-IQGAP3
Input
130-
250-
35-
Flag
IQGAP3
HA
IP: Flag (Axin1)
130-
250-
35-
Flag
IQGAP3
HA
1 0.70 0.54 0.43
HA/Flag
F
HEK293T
kDa
- + ++ +++
Myc-IQGAP3
Input
130-
250-
35-
Axin1
Myc
CK1α
IP: Axin1
130-
250-
35-
Axin1
Myc
CK1α
1 0.82 0.61 0.48
CK1α/Axin1

Fig. 5. IQGAP3 expression reduces Axin1-CK1α interaction. (A) Immunoblot of endogenous IQGAP3 immunoprecipitation using an IQGAP3-specific antibody (1:100) and Mouse IgG as a control, with 1 mg of HEK293 cell lysate. Samples were subjected to SDS-PAGE (7.5%) followed by immunoblotting using the indicated antibodies. (B) HEK293T cells were exposed to Wnt3a conditioned medium at different time points as indicated. Stimulated lysates were subjected to immunoprecipitation using an Axin1-specific antibody and Rabbit IgG as control and were subjected to SDS-PAGE (7.5%) followed by immunoblotting using the indicated antibodies. (C) HEK293T cells were exposed to Wnt3a conditioned medium at different time points as indicated. Stimulated lysates were subjected to IQGAP3 immunoprecipitation using Myc-Tag antibody and Mouse IgG as control and were subjected to SDS-PAGE (7.5%) followed by immunoblotting using the indicated antibodies. (D) Immunoblot of Flag-Immunoprecipitated protein expressing HA-Axin1 C-terminal truncations with Flag-IQGAP3 to map the IQGAP3 binding site within Axin1. Samples were subjected to SDS-PAGE (7.5%) followed by immunoblotting using the indicated antibodies. (E) IQGAP3 reduced exogenous Axin1-CK1 interaction. HEK293T cells expressing Flag-Axin1 were transfected with limiting amounts of HA-CK1α and increasing amounts of Myc-IQGAP3 (5μg/10μg/15μg) as indicated, and the lysates were subjected to anti-Flag immunoprecipitation. Samples were subjected to SDS-PAGE (7.5%) followed by immunoblotting using the indicated antibodies. The relative immunoblot bands of HA and Flag (HA/Flag) from the immunoprecipitation membrane were quantified by densitometry. (F) IQGAP3 reduced endogenous Axin1-CK1 interaction. HEK293T cells were transfected with increasing amounts of Myc-IQGAP3 (5μg/10μg/15μg) as indicated, and the lysates were subjected to anti-Axin1 immunoprecipitation. Samples were subjected to SDS-PAGE (10%) followed by immunoblotting using the indicated antibodies. The relative immunoblot bands of CK1α and Axin1 (CK1α/Axin1) from the immunoprecipitation membrane were quantified by densitometry.

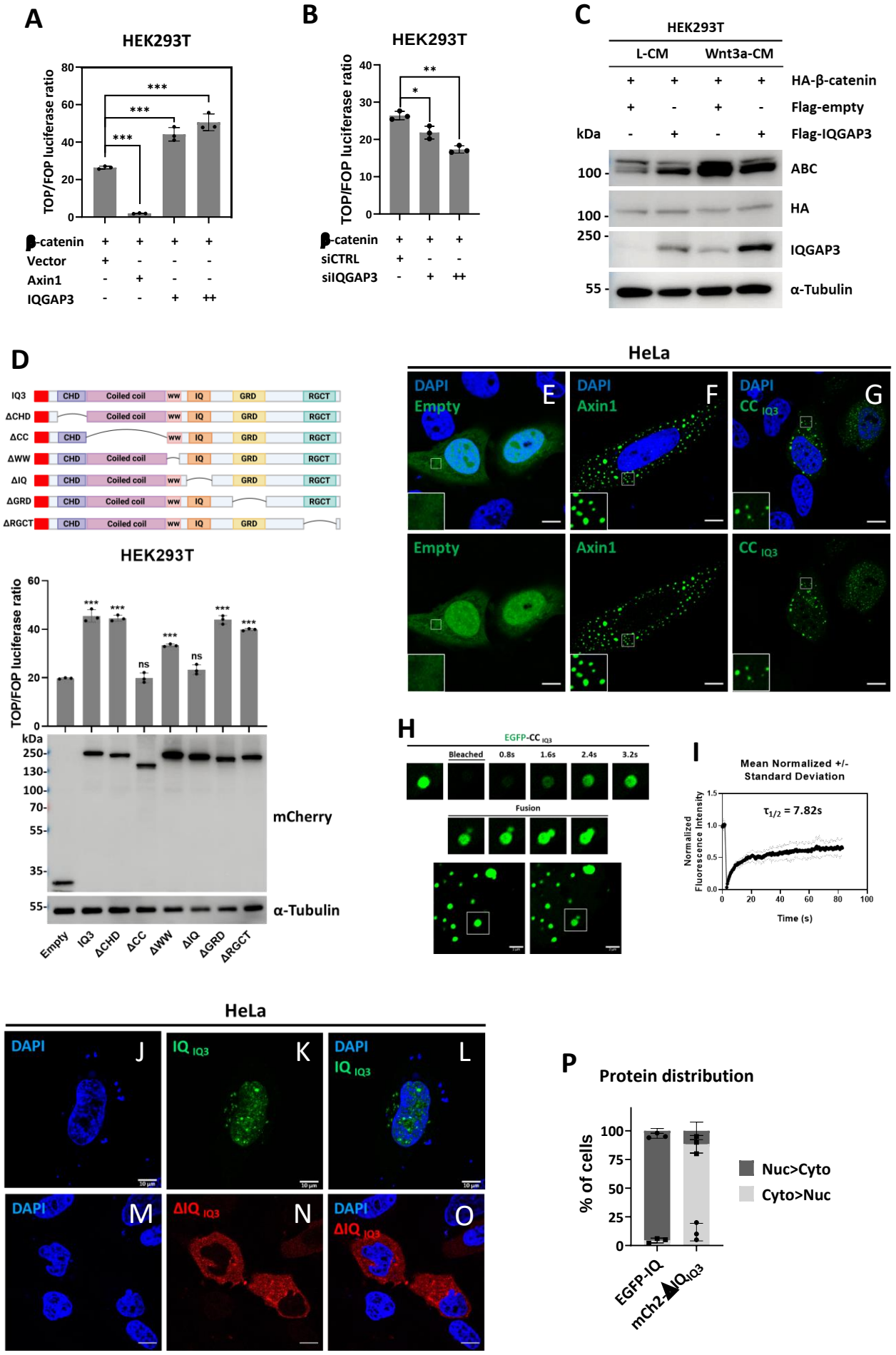
A
HEK293T
TOP/FOP luciferase ratio
β-catenin
Vector
Axin1
IQGAP3
B
HEK293T
TOP/FOP luciferase ratio
β-catenin
siCTRL
siIQGAP3
C
HEK293T
L-CM
Wnt3a-CM
HA-β-catenin
Flag-empty
Flag-IQGAP3
kDa
ABC
HA
IQGAP3
α-Tubulin
D
IQ3
ΔCHD
ΔCC
ΔWW
ΔIQ
ΔGRD
ΔRGCT
CHD
Coiled coil
WW
IQ
GRD
RGCT
HEK293T
TOP/FOP luciferase ratio
mCherry
α-Tubulin
Empty
IQ3
ΔCHD
ΔCC
ΔWW
ΔIQ
ΔGRD
ΔRGCT
HeLa
DAPI
Empty
Axin1
CC IQ3
E
F
G
H
EGFP-CC IQ3
Bleached
0.8s
1.6s
2.4s
3.2s
Fusion
I
Mean Normalized +/- Standard Deviation
Normalized Fluorescence Intensity
Time (s)
HeLa
DAPI
IQ IQ3
ΔIQ IQ3
J
K
L
M
N
O
P
Protein distribution
% of cells
Nuc>Cyto
Cyto>Nuc
EGFP-IQ
mCh2-ΔIQ IQ3

Fig. 6. IQGAP3 promotes β-catenin activity through its CC and IQ domains. (A) TOPFlash assay of β-catenin co-overexpression with Axin1 or increasing IQGAP3 (300μg, 600μg) in HEK293T cells. The data is representative of three independent experiments. Student's t test was performed, with $*p < 0.05$, $**p < 0.01$, and $***p < 0.001$. (B) TOPFlash assay of β-catenin co-overexpression with siControl or increasing siIQGAP3 (20nM, 50nM) in HEK293T cells. The data is representative of three independent experiments. Student's t test was performed, with $*p < 0.05$, $**p < 0.01$, and $***p < 0.001$. (C) Immunoblot of IQGAP3 overexpression with and without Wnt3a conditioned media treatment. The data is representative of three independent experiments. (D) TOPFlash and Immunoblot assays of β-catenin overexpression with a series of IQGAP3 domain deletions. The data is representative of three independent experiments. HeLa cells transfected with (E) EGFP-empty, (F) EGFP-Axin1, and (G) EGFP-CC. Scale bars, 10 μm. (H) HeLa cells were transfected with EGFP-CC, subjected to FRAP bleaching, and observed for recovery and fusion events. Scale bars, 2μm. (I) Mean normalized standard deviation of FRAP recovery of 10 bleached EGFP-CC condensates, half time of recovery ($\tau 1/2$) = 7.82s. HeLa cells transfected with (J-L) EGFP-IQ domain and (M-O) mCherry2-IQGAP3ΔIQ. Scale bars, 10 μm. (P) Percentile of cell count for protein distribution, cells with higher nuclear intensity were counted as Nuclear > Cytosol (Nuc > Cyto), vice versa. Cell count for protein distribution, 50 cells per sample. Representative data were collected and are expressed as the mean ± SD from three independent experiments (n=3).

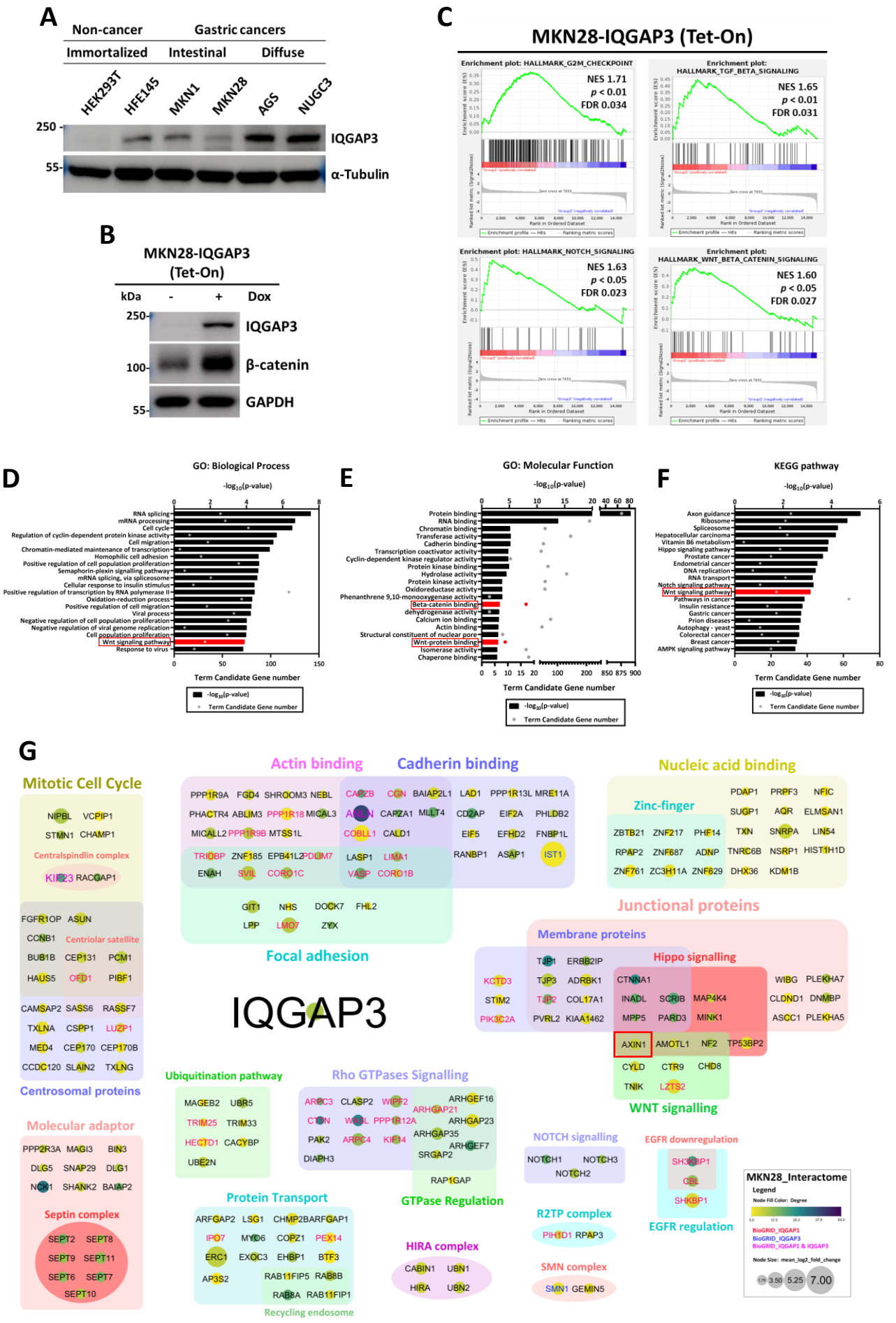
A
Non-cancer
Gastric cancers
Immortalized
Intestinal
Diffuse
HEK293T
HFE145
MKN1
MKN28
AGS
NUGC3
250
55
IQGAP3
α-Tubulin
B
MKN28-IQGAP3
(Tet-On)
kDa
-
+
Dox
250
100
55
IQGAP3
β-catenin
GAPDH
C
MKN28-IQGAP3 (Tet-On)
Enrichment plot: HALLMARK_G2M_CHECKPOINT
NES 1.71
p < 0.01
FDR 0.034
Enrichment plot: HALLMARK_TGF_BETA_SIGNALING
NES 1.65
p < 0.01
FDR 0.031
Enrichment plot: HALLMARK_NOTCH_SIGNALING
NES 1.63
p < 0.05
FDR 0.023
Enrichment plot: HALLMARK_WNT_BETA_CATENIN_SIGNALING
NES 1.60
p < 0.05
FDR 0.027
D
GO: Biological Process
-log10(p-value)
RNA splicing
mRNA processing
Cell cycle
Regulation of cyclin-dependent protein kinase activity
Cell migration
Chromatin-mediated maintenance of transcription
Homophilic cell adhesion
Positive regulation of cell population proliferation
Semaphorin-plexin signalling pathway
mRNA splicing, via spliceosome
Cellular response to insulin stimulus
Positive regulation of transcription by RNA polymerase II
Oxidation-reduction process
Positive regulation of cell migration
Viral process
Negative regulation of cell population proliferation
Negative regulation of viral genome replication
Cell population proliferation
Wnt signaling pathway
Response to virus
Term Candidate Gene number
-log10(p-value)
Term Candidate Gene number
E
GO: Molecular Function
-log10(p-value)
Protein binding
RNA binding
Chromatin binding
Transferase activity
Cadherin binding
Transcription coactivator activity
Cyclin-dependent kinase regulator activity
Protein kinase binding
Hydrolase activity
Protein kinase activity
Oxidoreductase activity
Phenanthrene 9,10-monooxygenase activity
Beta-catenin binding
dehydrogenase activity
Calcium ion binding
Actin binding
Structural constituent of nuclear pore
Wnt-protein binding
Isomerase activity
Chaperone binding
Term Candidate Gene number
-log10(p-value)
Term Candidate Gene number
F
KEGG pathway
-log10(p-value)
Axon guidance
Ribosome
Spliceosome
Hepatocellular carcinoma
Vitamin B6 metabolism
Hippo signaling pathway
Prostate cancer
Endometrial cancer
DNA replication
RNA transport
Notch signaling pathway
Wnt signaling pathway
Pathways in cancer
Insulin resistance
Gastric cancer
Prion diseases
Autophagy - yeast
Colorectal cancer
Breast cancer
AMPK signaling pathway
Term Candidate Gene number
-log10(p-value)
Term Candidate Gene number
G
Mitotic Cell Cycle
NIPBL VCPIP1
STMN1 CHAMP1
Centralspindlin complex
KIF23 RACGAP1
FGFR1OP ASUN
CCNB1 Centriolar satellite
BUB1B CEP131 PCM1
HAUS5 OFD1 PIBF1
CAMSAP2 SASS6 RASSF7
TXLNA CSPP1 LUZP1
MED4 CEP170 CEP170B
CCDC120 SLAIN2 TXLNG
Centrosomal proteins
Molecular adaptor
PPP2R3A MAGI3 BIN3
DLG5 SNAP29 DLG1
NCK1 SHANK2 BAIAP2
Septin complex
SEPT2 SEPT8
SEPT9 SEPT11
SEPT6 SEPT7
SEPT10
Actin binding
Cadherin binding
PPP1R9A FGD4 SHROOM3 NEBL
PHACTR4 ABLIM3 PPP1R18 MICAL3
MICALL2 PPP1R9B MTSS1L
TRIOBP ZNF185 EPB41L2 PDLIM7
ENAH SVIL CORO1C
CADPB CGN BAIAP2L1 LAD1 PPP1R13L MRE11A
AMSH CAPZA1 MLLT4 CDC42AP EIF2A PHLDB2
COBLL1 CALD1 EIF5 EFHD2 FNBP1L
LASP1 LIMA1 RANBP1 ASAP1 IST1
VASP CORO1B
GIT1 NHS DOCK7 FHL2
LPP LMO7 ZYX
Focal adhesion
IQGAP3
Nucleic acid binding
Zinc-finger
PDAP1 PRPF3 NFIC
SUGP1 AQR ELMSAN1
ZBTB21 ZNF217 PHF14 TXN SNRPA LIN54
RPAP2 ZNF687 ADNP TNRC6B NSRP1 HIST1H1D
ZNF761 ZC3H11A ZNF629 DHX36 KDM1B
Junctional proteins
Membrane proteins
Hippo signalling
TJP1 ERBB2IP
KCTD3 TJP3 ADRBK1 CTNNA1 WIBG PLEKHA7
STIM2 TJP2 COL17A1 INADL SCRIB MAP4K4 CLDND1 DNMBP
PIK3C2A PVRL2 KIAA1462 MPP5 PARD3 MINK1 ASCC1 PLEKHA5
AXIN1 AMOTL1 NF2 TP53BP2
CYLD CTR9 CHD8
TNIK LZTS2
WNT signalling
Ubiquitination pathway
MAGEB2 UBR5
TRIM25 TRIM33
HECTD1 CACYBP
UBE2N
Rho GTPases Signalling
ARHGEF16
ARHGAP21
ARHGAP23
ARHGAP35
ARHGEF7
SRGAP2
RAP1GAP
GTPase Regulation
NOTCH signalling
NOTCH1 NOTCH3
NOTCH2
EGFR downregulation
SH3C2P1
CBL
SHKBP1
EGFR regulation
Protein Transport
ARFGAP2 LSG1 CHMP2B ARFGAP1
IPO7 MYO6 COPZ1 PEX14
ERC1 EXOC3 EHBP1 BTF3
AP3S2 RAB11FIP5 RAB8B
RAB8A RAB11FIP1
Recycling endosome
HIRA complex
CABIN1 UBN1
HIRA UBN2
R2TP complex
PIH1D1 RPAP3
SMN complex
SMN1 GEMIN5
MKN28_Interactome
Legend
Node Fill Color: Degree
BioGRID_IQGAP1
BioGRID_IQGAP3
BioGRID_IQGAP1 & IQGAP3
Node Size: mean_log2_fold_change
3.50
5.25
7.00

Fig. 7. IQGAP3 overexpression increases β-catenin levels in MKN28 cells. (A) Immunoblot of non-cancer/immortalized (HEK293T and HFE145) and gastric cancer cell lines (MKN1, AGS, and NUGC3). Samples were subjected to SDS-PAGE (7.5%) followed by immunoblotting using the indicated antibodies. (B) Immunoblot of MKN28 cells expressing doxycycline-inducible 3×Flag-IQGAP3. Samples were subjected to SDS-PAGE (7.5%) followed by immunoblotting using the indicated antibodies. (C) GSEA data from RNA-seq of IQGAP3 overexpression in MKN28 cells, showing top 4 pathways. (D) Gene ontology: Biological Process Enrichment histogram of RNA-seq data from IQGAP3 overexpression in MKN28 cells. Wnt Signaling pathway represented with red bar. (E) Gene ontology: Molecular function Enrichment histogram of RNA-seq data from IQGAP3 overexpression in MKN28 cells. Wnt-protein and beta-catenin binding are represented with red bars. (F) KEGG pathway Enrichment histogram of RNA-seq data from IQGAP3 overexpression in MKN28 cells. Wnt Signaling pathway represented with red bar. (G) IQGAP3 interactome mapped from MKN28 cells stably expressing doxycycline-inducible TurboID-IQGAP3 (Fold change ≥ 2, p-value ≤ 0.05), node size represents log2 fold change and node color denote degree distribution, label color denotes: interactions found only in IQGAP1 Biogrid interactome database (red); interactions found only in IQGAP3 Biogrid interactome database (blue); and interactions found in both IQGAP1 and IQGAP3 Biogrid interactome database (purple), Created with Cytoscape.

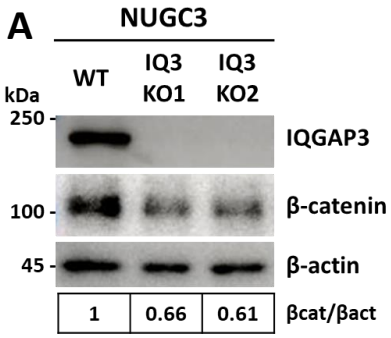
A
NUGC3
WT
IQ3 KO1
IQ3 KO2
kDa
250
100
45
IQGAP3
β-catenin
β-actin
1
0.66
0.61
βcat/βact

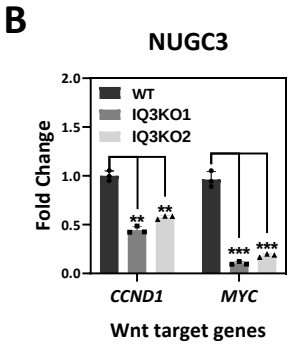
B
NUGC3
WT
IQ3KO1
IQ3KO2
Fold Change
2.0
1.5
1.0
0.5
0.0
CCND1
MYC
Wnt target genes

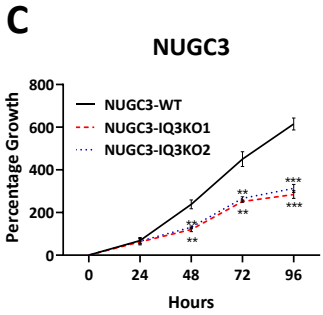
C
NUGC3
NUGC3-WT
NUGC3-IQ3KO1
NUGC3-IQ3KO2
Percentage Growth
800
600
400
200
0
0
24
48
72
96
Hours

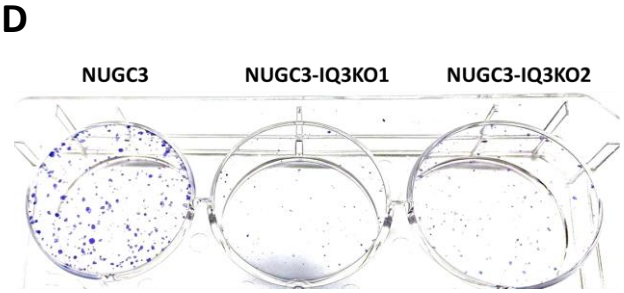
D
NUGC3
NUGC3-IQ3KO1
NUGC3-IQ3KO2

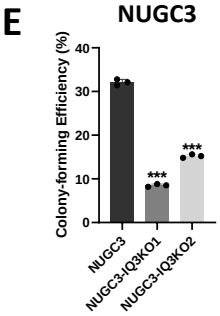
E
NUGC3
Colony-forming Efficiency (%)
40
30
20
10
0
NUGC3
NUGC3-IQ3KO1
NUGC3-IQ3KO2

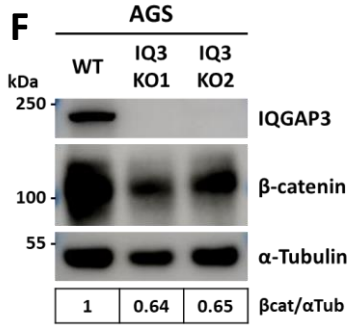
F
AGS
WT
IQ3 KO1
IQ3 KO2
kDa
250
100
55
IQGAP3
β-catenin
α-Tubulin
1
0.64
0.65
βcat/αTub

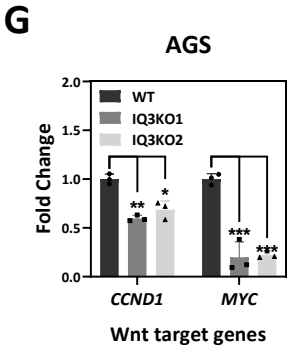
G
AGS
WT
IQ3KO1
IQ3KO2
Fold Change
2.0
1.5
1.0
0.5
0.0
CCND1
MYC
Wnt target genes

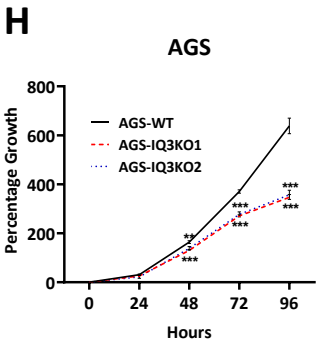
H
AGS
AGS-WT
AGS-IQ3KO1
AGS-IQ3KO2
Percentage Growth
800
600
400
200
0
0
24
48
72
96
Hours

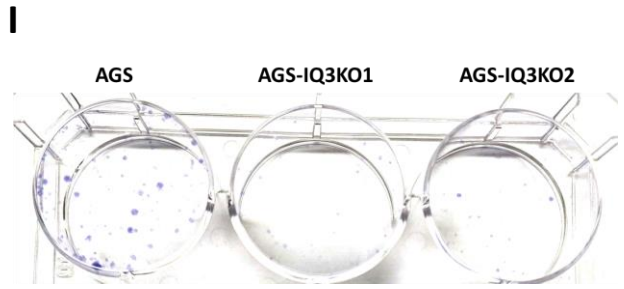
I
AGS
AGS-IQ3KO1
AGS-IQ3KO2

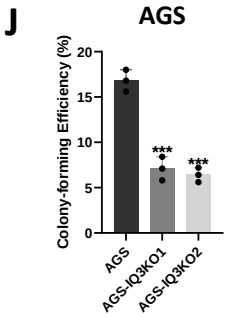
J
AGS
Colony-forming Efficiency (%)
20
15
10
5
0
AGS
AGS-IQ3KO1
AGS-IQ3KO2

Fig. 8. Loss of IQGAP3 reduces β-catenin levels in NUGC3 and AGS cells. (A) Immunoblot of NUGC3 wild-type and IQGAP3 CRISPR knock-out clones. Samples were subjected to SDS-PAGE (7.5%) followed by immunoblotting using the indicated antibodies. The relative immunoblot bands of β-catenin and β-actin (βcat/βact) were quantified by densitometry. (B) NUGC3 cells were lysed, and RNA collected were converted to cDNA and subjected to RT-PCR to quantify the amount of Wnt target genes *CCND1* and *MYC.* Representative data were collected and are expressed as the mean ± SD from three independent experiments. Student's t test was performed, with $*p < 0.05$, $**p < 0.01$, and $***p < 0.001$. (C) XTT Cell Proliferation Assay of NUGC3 wild-type and IQGAP3 CRISPR knock-out clones. Representative data were collected and are expressed as the mean % growth ± SD from three independent experiments. Two-way ANOVA was performed, with $*p < 0.05$, $**p < 0.01$, and $***p < 0.001$. (D) Clonogenic Assay of NUGC3 wild-type and IQGAP3 CRISPR knock-out clones. (E) Colony-Forming Efficiency (%) of NUGC3 wild-type and IQGAP3 CRISPR knock-out clones. (F) Immunoblot of AGS wild-type and IQGAP3 CRISPR knock-out clones. Image is best representative of three independent experiments. Samples were subjected to SDS-PAGE (7.5%) followed by immunoblotting using the indicated antibodies. The relative immunoblot bands of β-catenin and α-Tubulin (βcat/αTub) were quantified by densitometry. (G) AGS cells were lysed, and RNA collected were converted to cDNA and subjected to RT-PCR to quantify the amount of Wnt target genes *CCND1* and *MYC.* Representative data were collected and are expressed as the mean ± SD from three independent experiments. Student's t test was performed, with $*p < 0.05$, $**p < 0.01$, and $***p < 0.001$. (H) XTT Cell Proliferation Assay of AGS wild-type and IQGAP3 CRISPR knock-out clones. Representative data were collected and are expressed as the mean % growth ± SD from three independent experiments. Two-way ANOVA was performed, with $*p < 0.05$, $**p < 0.01$, and $***p < 0.001$. (I) Clonogenic Assay of AGS wild-type and IQGAP3 CRISPR knock-out clones. (J) Colony-Forming Efficiency (%) of AGS wild-type and IQGAP3 CRISPR knock-out clones.

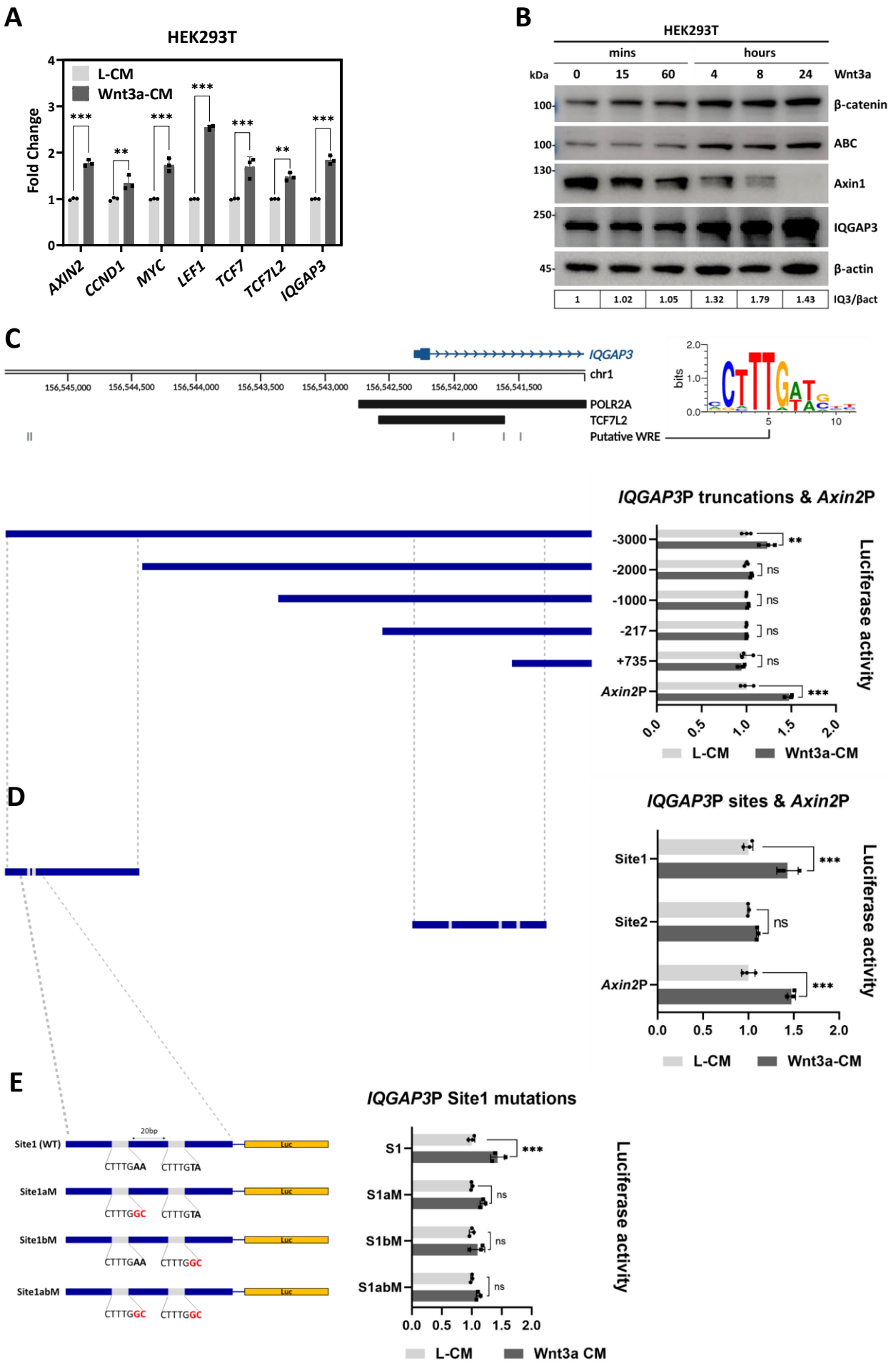
A
HEK293T
L-CM
Wnt3a-CM
Fold Change
AXIN2
CCND1
MYC
LEF1
TCF7
TCF7L2
IQGAP3
B
HEK293T
mins
hours
kDa
0
15
60
4
8
24
Wnt3a
β-catenin
ABC
Axin1
IQGAP3
β-actin
1
1.02
1.05
1.32
1.79
1.43
IQ3/βact
C
IQGAP3
chr1
POLR2A
TCF7L2
Putative WRE
bits
IQGAP3P truncations & Axin2P
-3000
-2000
-1000
-217
+735
Axin2P
ns
Luciferase activity
L-CM
Wnt3a-CM
D
IQGAP3P sites & Axin2P
Site1
Site2
Axin2P
E
Site1 (WT)
Site1aM
Site1bM
Site1abM
20bp
Luc
CTTTGAA
CTTTGTA
CTTTGGC
IQGAP3P Site1 mutations
S1
S1aM
S1bM
S1abM
L-CM
Wnt3a CM

Fig. 9. IQGAP3 is a target of Wnt signaling, sustains Wnt signaling via a positive feedback loop. (A) HEK293T cells were treated with wnt3a conditioned media supplemented with 100ng/ml of rhWnt3a. Cells were harvested, and the RNA collected were converted to cDNA and subjected to RT-PCR to quantify the amount of *AXIN2, CCND1, MYC, LEF1, TCF7, TCF7L2* and *IQGAP3* transcripts levels. (B) Time-course of HEK293T cells treated with Wnt3a conditioned media supplemented with 100ng/ml of rhWnt3a. Image is best representative of three independent experiments. Samples were subjected to SDS-PAGE (7.5%) followed by immunoblotting using the indicated antibodies. The relative immunoblot bands of IQGAP3 and β-actin (IQ3/βact) were quantified by densitometry. (C) Luciferase assay of 5' truncation of IQGAP3 promoter region upon treatment with L-cells conditioned or wnt3a conditioned media. (D) Luciferase assay of Site1 and Site2 within the IQGAP3 promoter region upon treatment with L-cells conditioned or wnt3a conditioned media. (E) Luciferase assay of Site1, Site1a mutant, Site1b mutant and Site1ab mutant upon treatment with L-cells conditioned or wnt3a conditioned media. All the above data are representative of three independent experiments.

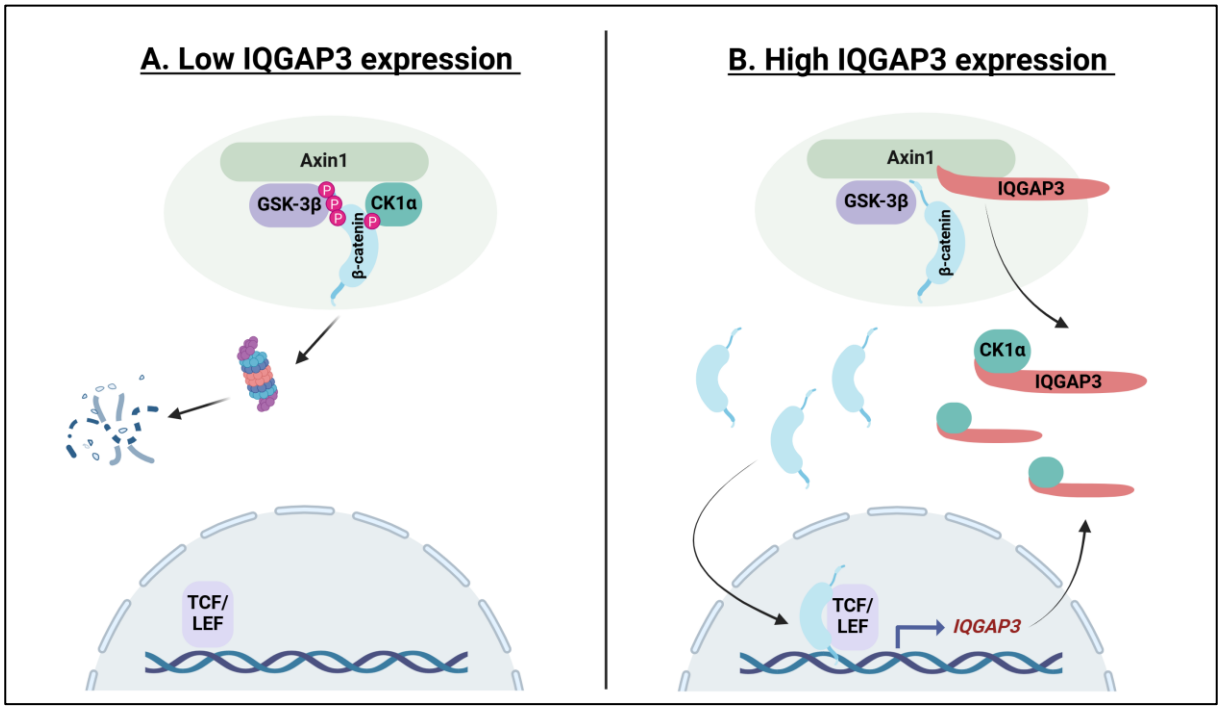
A. Low IQGAP3 expression
Axin1
GSK-3β
CK1α
P
β-catenin
TCF/
LEF
B. High IQGAP3 expression
Axin1
IQGAP3
GSK-3β
β-catenin
CK1α
IQGAP3
TCF/
LEF
IQGAP3

Fig. 10: Proposed model for IQGAP3 role in Wnt signalling. We proposed that In IQGAP3-low cells (A), the destruction complex phosphorylates β-catenin, targeting it for degradation. Meanwhile, in IQGAP3-high cells (B), IQGAP3 competes with CK1α for binding to Axin1 or sequesters it away from Axin1 or both, thus, inhibiting CK1α-mediated β-catenin phosphorylation. This inhibition leads to the accumulation of β-catenin, which promotes the expression of Wnt target genes, including IQGAP3, Created with BioRender.com.